Structural Change of Troponin C Molecule upon Ca^{2+} or Mg^{2+} Binding Studied by Solution X-ray Scattering Technique

By

Tetsuro Fujisawa

DEPARTMENT OF BIOPHYSICAL ENGINEERING

GRADUATE DIVISION

FACULTY OF ENGINEERING SCIENCE

OSAKA UNIVERSITY

MARCH, 1989

ABSTRACT

Troponin is the Ca^{2+}-binding protein which regulates the interaction between myosin and actin in skeletal muscle of vertebrate, and troponin C is a Ca^{2+}-binding subunit of troponin. Herzberg and James in 1985 and Sundaralingam et al. in 1985 did crystal structure analysis of troponin C attached by two Ca^{2+} ions in muscles of turkey and chicken and showed that the molecule is dumbbell-shaped, with two distinct domains connected by a long helix. The present study was undertaken to examine whether troponin C has the same shape in solution as in crystal and how Ca^{2+} and/or Mg^{2+} bindings affect the structure. The solution X-ray scattering method was utilized for the study with the synchrotron radiation as a strong X-ray source. Dilute solution of rabbit skeletal troponin C of 2-10 mg/ml was used, for which no indication of aggregation of troponin C molecule was found. Two tryptic fragments of troponin C, i.e., TR2C (C-terminal domain) and TR1C (N-terminal domain) were studied as well. Obtained results are summarized as follows:

1. The distance distribution function calculated from the solution scattering data showed two peaks, suggesting the dumbbell structure irrespective of binding of Ca^{2+} and Mg^{2+}. The radius of gyration Rg of troponin C decreased from 27.8 Å to 22.6 Å increasing number of bound Ca^{2+} ions.
2. The average radius of gyration of the domain $\overline{Rg}_{N,C}$ and separation of the centers of the two domains r_{NC} were estimated from the X-ray scattering data of troponin C itself. $\overline{Rg}_{N,C}$ decreased from 15.4 Å to 14.8 Å and r_{NC}

decreased from 46.3 Å to 34.5 Å upon Ca^{2+} binding.

3. Solution X-ray scattering studies of the tryptic fragments of troponin C revealed that Rg_C (Rg of TR2C) is 17.0 Å and Rg_N (Rg of TR1C) is 14.0 Å in the absence of Ca^{2+}. This data indicates that the C-terminal domain is considerably expanded in the absence of Ca^{2+}, whereas the N-terminal domain has a relatively compact structure even in the presence of Ca^{2+}. Rg_C decreased to 14.7 Å upon Ca^{2+} binding. These observations are in accordance with an increase of α-helicity measured through circular dichroism (Kawasaki and van Eerd, 1972); and with results of NMR (Leavis et al., 1982) and fluorescence (van Eerd and Kawasaki, 1973) studies that the structure of troponin C becomes more ordered upon Ca^{2+} binding.
4. Binding of Mg^{2+} to the high affinity sites causes a structural change analogous to that of Ca^{2+}.
5. Comparison of the present results with that of the crystal structure analysis shows that overall structure of troponin C in solution is similar to that in the crystal, although the size of each domain in solution is a little larger than in crystal.

CONTENTS

ABBREVIATIONS USED IN THIS PH.D. THESIS

Tn-C: troponin-C, Tn-I: troponin-I, Tn-T: troponin-T

Ca_0Tn-C: Tn-C in the absence of Ca^{2+} and Mg^{2+}

Ca_2Tn-C: Tn-C at pCa 6.5 where one Tn-C molecule carries two Ca^{2+} in high affinity sites

Ca_4Tn-C: Tn-C at pCa 4.0 where one Tn-C molecule carries four Ca^{2+}

Mg_2Ca_0Tn-C: Ca^{2+}-free Tn-C in the presence of Mg^{2+} where Tn-C carries two Mg^{2+} in high affinity sites

Mg_2Ca_2Tn-C: Tn-C at pCa 4.0 in the presence of Mg^{2+} where Tn-C carries two Mg^{2+} in high affinity sites and two Ca^{2+} in high affinity sites.

EDTA: ethylenediamine tetraacetic acid

NMR: nuclear magnetic resonance, CD: circular dichroism

PMR: proton magnetic resonance

MOPSO: 3-(N-Morpholino)-2-hydroxypropane-sulfonic acid

UV: ultra violet, MW: molecular weight

SDS: sodium dodecyl sulfate

$S_{20,w}$: sedimentation coefficient

PAGE: polyacrylamide gel electrophoresis

TR1C: tryptic fragment which contains residues from 9 to 84 of native Tn-C

TR2C: tryptic fragment which contains residues from 89-159 of native Tn-C

EGTA: ethylenebis(oxyethylenenitrilo) tetraacetic acid

SOXS: solution X-ray scattering

MAXS: modulate-angle X-ray scattering

INTRODUCTION

In INTRODUCTION the author describes the backgrounds of structural studies of troponin C measured by other methods and then explain the aim of this study.

1. The Biological Role of Troponin and Its Subunits

The activation of muscle contraction, especially in the vertebrate, is triggered by the binding of Ca^{2+} to Ca^{2+}-binding protein called troponin. Troponin is located on thin filament and regulates the interaction between myosin and actin. In the absence of Ca^{2+}, troponin inhibits the activation of actin induced through the ATP hydrolysis by myosin (1). Troponin consists of three subunits, Tn-C, Tn-I and Tn-T. Tn-C is the Ca^{2+} binding subunit; Tn-T, the tropomyosin binding subunit, serves as a link to attach the troponin complex to the thin filament *via* tropomyosin ; Tn-I, the inhibitory subunit, prevents ATPase activity in the system of tropomyosin and actomyosin by itself (2,3). This thesis deals with Tn-C, which serves as a key role in troponin.

2. The Properties of Tn-C

The determination of the amino acid sequence of Tn-C from rabbit skeletal muscle showed that it consists of a single polypeptide chain of 159 residues (4). Tn-C is a highly acidic protein containing a large number of asparatic and glutamic acid residues. It is negatively charged at neutral pH. Molecular weight of Tn-C is calculated from amino acid sequence to be

17,846. Potter and Gergely showed four Ca^{2+} binding sites (5). They are numbered from I to IV from the N-terminus. Sites III and IV are Mg^{2+}-competitive Ca^{2+} binding sites with high affinity (high affinity sites hereafter) and the other sites I and II are Ca^{2+}-specific binding sites with low affinity (low affinity sites hereafter). Leavis et al. used tryptic fragments of Tn-C and showed that two sites from the C-terminus are high affinity sites and two from low affinity are low affinity sites, respectively (6). Binding affinities are summarized in the Table 1 (5,6).

Table 1: Summaries of binding affinities for Ca^{2+} and Mg^{2+} of Tn-C and tryptic fragments

protein or peptides	sites	$K_{Ca\ in\ -Mg^{2+}}$	$K_{Ca\ in\ +Mg^{2+}}$	K_{Mg}
Tn-C	high affinity sites	2.1×10^{7}	2.8×10^{6}	$2\sim4\times10^{3}$
Tn-C	low affinity sites	3.2×10^{5}	1.1×10^{5}	———
TR1C (9-84)	low affinity sites	$<1.0\times10^{5}$	$<1.0\times10^{5}$	———
TR2C (89-159)	high affinity sites	5.0×10^{7}	———	2×10^{4}

3. Crystal Structure of Tn-C

There have been two reports on the three dimensional structure of Tn-C determined by X-ray crystallography (7-10). Two reports used Tn-C from different species from chicken and turkey but the results were identical. In crystalline state

both turkey and chicken Tn-C carries only two Ca^{2+} in excess Ca^{2+} medium. A schematic view of the turkey skeletal is cited from Herzberg and James on next page (9).

The C-terminus domain of high affinity sites (C-domain hereafter) and the N-terminus domain of low affinity sites (N-domain hereafter) are connected by a nine-turn α-helix and no contact exists between the two domains : a dumbbell structure. The N-domain includes the first 85 amino acids and the C- domain comprises residues from 97 to 162. The two Ca^{2+} are separated by 11.7 Å. The molecular length is 75 Å and each domain has a 25 Å diameter and the centers of the two domains are about 40 Å apart (10).

Ca^{2+}-binding loops in C-domain are termed 'EF-hand': the helix-loop-helix at right angles, assigned as Ca^{2+} binding region (11). The other Ca^{2+} binding protein which have the 'EF-hand' loop are known such as parvalbumin, intestinal Ca^{2+}-binding protein, and calmodulin. The dumbbell shape was also reported for calmodulin which is fully occupied by four Ca^{2+} in crystal (12).

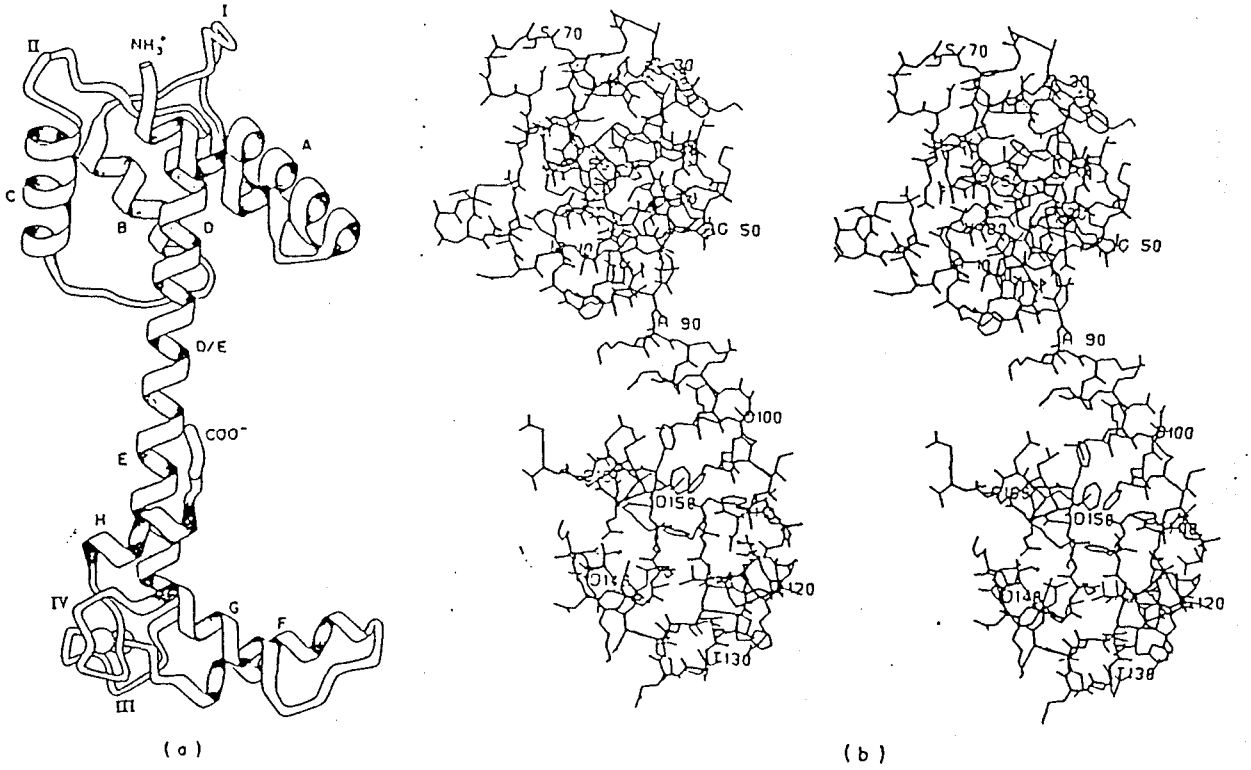

Figure 1: Crystalline structure of turkey skeletal Tn-C cited from Herzberg and James (7,9). (a) A ribbon representation of the polypeptide chain. (b) Stereoscopic representation of the whole molecule.

4. Structural Change of Tn-C upon Ca^{2+} or Mg^{2+} Binding

4.a. Structural Change of Tn-C upon Ca^{2+} Binding

It is a well known fact that binding of Ca^{2+} causes a considerable structural change of Tn-C and is supported by many spectroscopical studies and physical chemical analyses (1,2). The increase in circular dichroism in the 222-nm region $[\theta]_{222}$ indicate an increase in α-helical content. It increases from 36 % of Ca_0Tn-C to 48 % of Ca_2Tn-C. Further Ca^{2+} binding to Tn-C α-helical content becomes 52 % (13).

Table 2. Secondary structure of Tn-C determined from CD measurements

condition	α-helix (%)	β structure (%)	random-coil (%)
Ca_0Tn-C	36	14	50
Mg_2Ca_0Tn-C	48	14	38
Ca_4Tn-C	52	12	36
Mg_2Ca_2Tn-C	52	12	36

* These values are taken from Kawasaki et al. (14).

A general tightening of the structure is also supported by hydrodynamic data that show an increase in the $S_{20,w}$ (15-18) and a decrease in the viscosity of the Tn-C solution upon addition of Ca^{2+} (17).

NMR and PMR studies analyzed several resonance peaks of residues in N-domain and C-domain (19,20). Binding of Ca^{2+} to high affinity sites induced broadening of resonances assigned to

phenylalanine, leucine, and isoleusine residues in C-domain, which is indicative of increased restriction of movement and formation of hydrophobic cluster in C-domain. Changes of resonance of residues in N-domain suggests that a hydrophobic cluster exists irrespective of Ca^{2+} binding to N-domain. It also suggests that Ca^{2+} binding to N-domain results in the loss of hydrophobic contracts leading to the conformational change of a tightening of the pre-existing helices. Local conformational change is also detected by fluorescence probes attached to Tn-C and tyrosine fluorescence (1,2,21). These fluorescence studies also support the above scheme of structural change.

4.b. Structural change of Tn-C upon Mg^{2+} binding

Not only Ca^{2+} but also Mg^{2+} binds to the Tn-C molecule and cause the structural change. In the myofibril there are a few millimolars of Mg^{2+} and the Tn-C molecule is supposed to carry two Mg^{2+} ions in high affinity sites (22). The initiation of contraction events is parallel to the binding of Ca^{2+} to low affinity sites as well as the exchange of Mg^{2+} with Ca^{2+} in low affinity sites. The large conformational change of secondary structure was also observed in the addition of millimolar concentrations of Mg^{2+} to Ca^{2+}- and Mg^{2+}-free Tn-C (Ca_0Tn-C). CD measurement suggests that secondary structure of Tn-C with Mg^{2+} in high affinity sites is the same as that of Tn-C with Ca^{2+} (14). But the structure of Tn-C is believed to be a little different between Ca_2Tn-C and Mg_2Ca_0Tn-C. Thermostability of Mg_2Ca_0Tn-C is slightly lower than Ca_2Tn-C and NMR spectra and fluorescence around Cys-98 in C-domain were also different

(21,23).

5. Recent Studies of Tn-C Structure and its Structural Change

After the crystal structure of Tn-C was elucidated, many questions arose. The two most critical questions were:

The first question is "Does the Tn-C molecule have a dumbbell structure under the physiological conditions ?" Tn-C was crystallized in pH 5.0 (7-10). The difference in binding affinity between high affinity sites and low affinity sites disappeared under these conditions (24). Furthermore the distance between the two domains measured by fluorescence energy transfer methods varied with pH (25). Estimated distance was less than that in crystalline state; the distance between Tb^{3+} bound at low affinity sites and the probe attached at Cys-98 was 27 Å at pH 6.8 and >52 Å at pH 5.0, respectively. No contact between N- and C-domains in the crystal structure can not explain the interaction between N- and C-domains reported by various methods (6,19,26-29). It is now quite doubtful whether the structure in crystalline state is the same as that in physiological condition.

The other question is "How does the structure of Tn-C change upon Ca^{2+} or Mg^{2+} binding ?" ; There are two conflicting results concerning the structural change of troponin C. The first represented by CD measurements and other methods as described earlier indicated a large structural change upon Ca^{2+} binding. To the contrary recent two SAXS reports ruled out large structural change (30,31). Their Rg's did not change largely

upon Ca^{2+} or Mg^{2+} binding. The distance between two probes attached to Methionine-25 and Cystein-98 measured by fluorescence energy transfer methods remains unchanged (32,33). Since the results of the other SAXS reports were inadequate for the definitive conclusion, the complete SOXS studies are necessary in order to study structures of Tn-C in solution.

6. Aim of This Thesis

The SAXS method is very useful in studying the overall structure of a protein molecule under physiological conditions. Dr. Ueki *et al.* analyzed the SAXS profile of oligomeric protein in terms of "domain scattering" (34). The author developed his idea and analyzed the profiles by a new method which determines the physical parameters of the Tn-C structure (35). The Tn-C molecule however was reported to cause dimerization upon Ca^{2+} binding (36). The aggregation state of Tn-C was studied in dilute concentration range 2-10 mg/ml. Based on the obtained intrinsic SAXS profiles from Tn-C, the structural changes of Tn-C caused by Ca^{2+} and Mg^{2+} were investigated. Research on structural change of tryptic fragments of Tn-C was also performed.

EXPERIMENTAL PROCEDURES

1. Preparation of Tn-C

Troponin was prepared from white rabbit skeletal muscle according to the method of Wakabayashi (37). Experimental procedure is described below.

PREPARATION OF TROPONIN

Minced white muscle incubated in -4 ℃ salt-ice
↓
Wash with 0.3 liter of Gauber-Straub solution (0.3 M KCl, 0.15 M phosphate potassium buffer pH 6.5) against 100 g muscle
↓
After 30 minutes dialyze the solution with 1.2 liter water
↓
Wash three times by 0.3 liter of 0.05M KCl solution containing 0.3 mM $NaHCO_3$
↓
Wash twice by 0.3 liter of 0.3 mM $NaHCO_3$
↓
Add half volume of 1.2 M LiCl to the residues
↓
Centrifugalize 15 minutes 10,000 rpm
↓
The sediment was added an equal volume of 0.4 M LiCl
↓
Adjust pH of the sample to 4.5 by 1 N HCl and leave three hours (the pH was check every hour)
↓
Centrifugalize 15 minutes 10,000 rpm
↓
Adjust pH of the solution to 7.6
↓
Add 30 g of $(NH_4)_2SO_4$ to 100 ml of the supernatant
↓
Centrifugalize 30 minutes 10,000 rpm
↓
Add 20 ml of saturated $(NH_4)_2SO_4$ to 100 ml of supernatant
↓
Centrifugalize 30 minutes 10,000 rpm
↓
Dissolve the precipitate in a small amount of 1 mM $NaHCO_3$
↓
Dialyze against 0.3 mM $NaHCO_3$ through a night
↓
crude troponin (The amounts of solutions are for 100 g muscle)

Obtained troponin was separated into three components by the use of DEAE-Sephadex A-25 column chromatography in the presence of 6M urea (38). The troponin sample in $NaHCO_3$ was dialyzed against 6 M urea, 20 mM Tris-HCl (pH 8.0). The sample was applied to the column and separated into components by a linear gradient of 0-0.6 M KCl in 6 M urea, 20 mM Tris-HCl (pH 8.0). Tn-C was purified by DEAE-sephadex column chromatography until only one clear band could be seen in SDS PAGE.

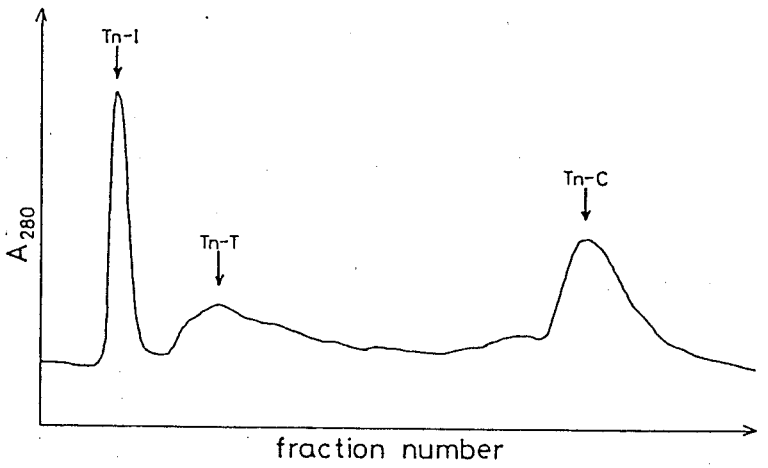

Figure 2: DEAE-Sephadex A-25 chromatography of troponin. Troponin was loaded on a column (3.5 x 20 cm) equilibrated with 6 M urea, 20 mM Tris-Hcl (pH 8.0). The column was eluted with a gradient of KCl to 0.6 M.

The distinct feature of the UV absorption spectrum of Tn-C is the five peaks at 276 nm, 268 nm, 265 nm, 259 nm, 253 nm and one shoulder at 282 nm. A typical absorption spectrum was shown below.

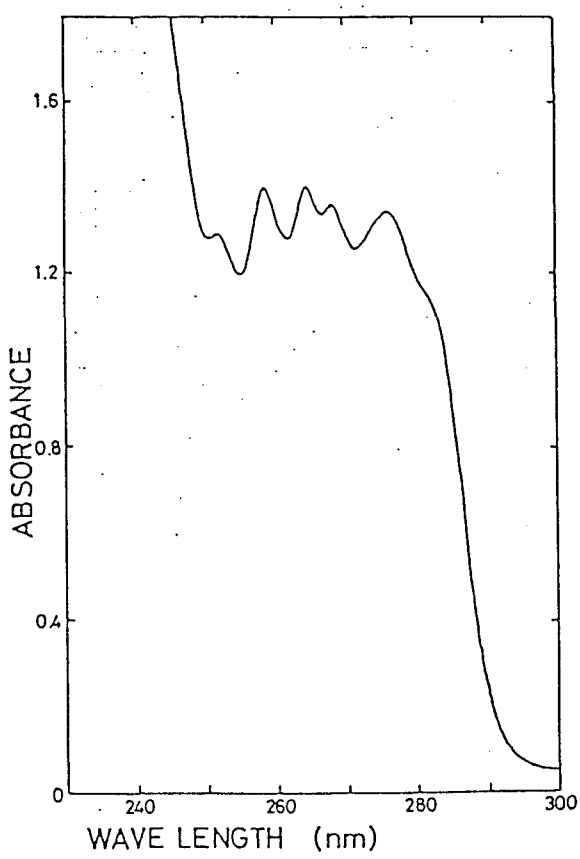

Figure 3: UV spectrum of Tn-C.

2. Preparation of Tryptic Fragments of Tn-C

Leavis et al. found that trypsin divides Tn-C into two fragments in the presence of Ca^{2+} (6). They are called TR1C and TR2C. TR1C (9-84) contains I and II sites, while TR2C (89-162) contains III and IV sites. Like the intact Tn-C molecule, TR2C has the same binding affinities for Ca^{2+} and Mg^{2+} (see Table 1). It is considered a good model for high affinity sites of Tn-C (6). TR1C and TR2C were purified according to the method of Tsalkova & Privalov (28).

Tryptic hydrolysis of Tn-C was carried out at 20℃ in a solution of 10 mM Tris-HCl (pH 8.0), 10 mM $CaCl_2$ with a substrate to enzyme molar ratio of 100:1. The digestion mixture contained degraded small fragments, trypsin and raw Tn-C together with the tryptic fragments. They were first purified on a Sephadex G50 column using 50 mM Tris-HCl (pH 8.2), 1 mM $CaCl_2$, 200 mM KCl as the eluent. The used fractions are indicated in Figure 4 (a).

Separation of TR1C and TR2C was done on a DEAE-Sephadex A-25 column with a 0.2 M to 0.5 M KCl gradient and several fraction were checked by SDS PAGE (Figure 4 (b)).

TR1C and TR2C have a characteristic UV absorption spectrum which resembles that of parvalbumin. The peptides were identified by electrophoresis in 10 % (w/v) polyacrylamide gels with 5 M Urea and SDS PAGE together with UV absorption spectra (39) (Figure 5).

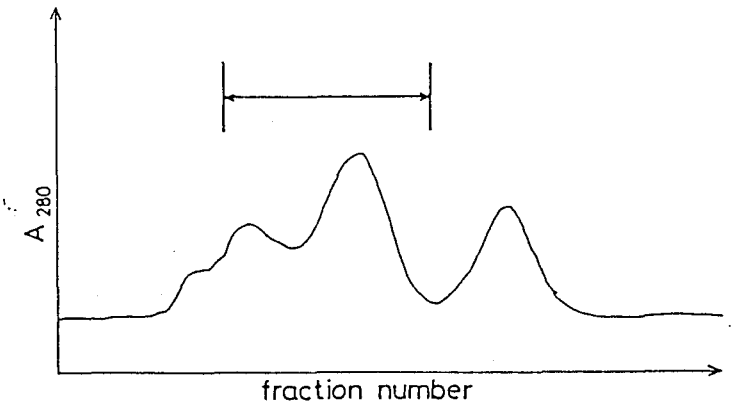

(a)

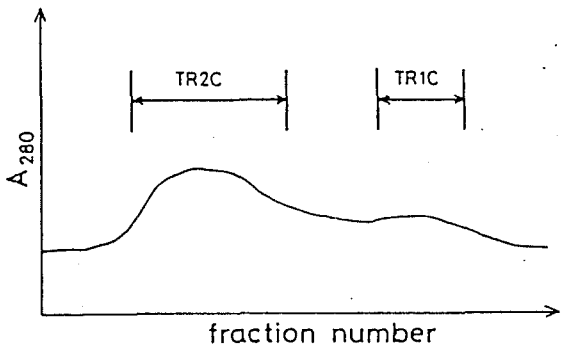

(b)

Figure 4 (a): Chromatographic profile of tryptic hydrolysates. The hydrates were loaded on a Sephadex G50 column (2.6 x 90 cm) and eluted with 50 mM Tris-HCl (pH 8.2), 1 mM $CaCl_2$, 200 mM KCl. The used fractions were indicated in the figure.
(b): Separation of TR1C and TR2C. Separation on a DEAE-Sephadex A25 column (3.5 x 15 cm) saturated with 50 mM-Tris-HCl (pH 8.2), 0.1 mM CaCl2, 200 mM KCl. Elusion from a 0.2 M to 0.5 M KCl gradient. The fractions were identified by SDS-PAGE.

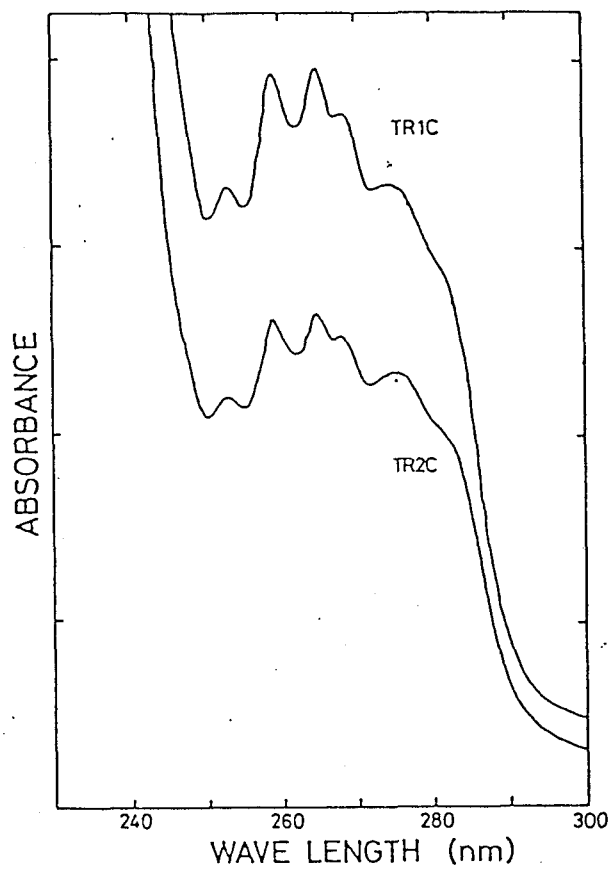

Figure 5: UV spectra of TR1C and TR2C.

3. Ca^{2+} and Mg^{2+} Binding to Tn-C and its Tryptic Fragments

Tn-C solution, bound by different amounts of Ca^{2+} or Mg^{2+}, was prepared as follows. First, the Tn-C solution was dialyzed exhaustively against a solution of 5 mM EDTA/KOH (pH 7.0) for 24 hours to remove Ca^{2+} and Mg^{2+}. After dialysis in distilled water, the Tn-C was dialyzed in a sample buffer. The sample buffer was 0.1 M KCl-10 mM MOPSO/KOH (pH 7.0), 2 mM EDTA for Mg^{2+}-free experiments. For Mg^{2+} binding experiments 2 mM EGTA was used instead of 2 mM EDTA.

This Ca^{2+}- and Mg^{2+}-free Tn-C solution was then concentrated with an ultrafiltration membrane CF50A (AMICON corp.) centrifuged 3,000 rpm for 10 minutes. The concentration was determined by ultraviolet absorption at 280 nm, $A_{280}^{10\ mg/ml} = 1.83$ (13).

Ca^{2+}-free TR1C and TR2C solution were obtained in the same manner as the Tn-C solution. The concentration was determined by ultraviolet absorption at 280 nm, $A_{280}^{1\ mg/ml} = 0.141$ for TR1C and $A_{280}^{1\ mg/ml} = 0.147$ for TR2C, respectively (6).

A very small amount of concentrated $CaCl_2$ or $MgCl_2$ solutions in buffer were added to the metal-free solution in order to achieve the desired ion concentrations. Free Ca^{2+} concentrations were pCa 6.5, pCa 4.0 for Ca_2Tn-C and Ca_4Tn-C, respectively. In the presence of Mg^{2+}, free Ca^{2+} concentration was pCa 4.0 for Mg_2Ca_2Tn-C. For Mg^{2+}-bound experiments the total concentration of $MgCl_2$ was 2 mM. The computer program for calculation of free Ca^{2+} concentration was written by Perrin and Sayce (40). The logarithmic association constants for Tn-C and, TR1C and TR2C were cited from Potter and Gergely (5), and Leavis et al. (6), respectively.

The pH of all the sample solutions was readjusted by adding a small amount of KOH solution.

For the SAXS experiments, concentration of solution were 2 mg/ml, 3 mg/ml, 4 mg/ml, 6 mg/ml, 8 mg/ml, 10 mg/ml for Tn-C, 2.84 mg/ml, 4.25 mg/ml, 5.67 mg/ml, 7.09 mg/ml for TR1C and 8.16 mg/ml, 9.05 mg/ml, 9.56 mg/ml, 10.8 mg/ml, 12.3 mg/ml, 13.6 mg/ml, TR2C. For the MAXS experiments, a 20 mg/ml of Tn-C concentration and 34.1 mg/ml of TR2C concentration were employed

in order to record the SOXS profile in moderate-angle region with accuracy.

4. Preparation of Lysozyme

Chicken egg-white lysozyme was used as a reference protein for molecular weight determination of Tn-C. Lysozyme was obtained from Merck & Co., Inc. (lot.5281). Lyophilized powder of lysozyme was dialyzed against a solution of 150 mM NaCl and 40 mM sodium acetate, pH 3.8. The protein concentration was determined spectrophotometrically using $E_{282}^{1mg/ml} = 2.64$ (41).

For SAXS experiments concentration of solution were 3.25 mg/ml, 6.5 mg/ml and 11.0 mg/ml for lysozyme.

5. SAXS Optics

A dilute solution of small protein gives a quite week scattering intensity and the background-corrected intensity tends to be very noisy. It was difficult to get SAXS profiles from Tn-C (molecular weight is about 18,000) and tryptic fragments(molecular weight is about 8,500) with low protein concentrations in a moderate signal to background ratio by using an ordinary X-ray generator. Thus, the use of intense synchrotron radiation (SR) with improved SAXS optics is essential to obtain less noisy profile. SAXS profiles for Tn-C solutions were recorded with SR from a 2.5 GeV storage ring at Photon Factory of the National Laboratory for High-Energy Physics, Tsukuba.

The optics consist of double flat crystals, a toroidal mirror, and four slit systems (42,43). The incident X-rays

were monochromatized through double monochromators, which were tuned to a wavelength of λ = 1.48 Å. The layout of the optical elements is shown in Figure 6 (a).

The camera is installed in chambers filled with helium gas and the beam path from the mirror is evacuated. The parasitic scattering from the mirror was eliminated by the third and fourth slits. The aperture of the third slit was 1.25 mm. From the downstream vacuum window, all parts are in a safety hatch. The detailed installation of optical elements near the sample holder in the hatch is shown in Figure 6 (b). The position of the fourth slit, sample holder and beam stop was remote controlled. Sample to detector length was 80 cm. The sample thickness was 1.3 mm, the effect of X-ray absorption of Ca^{2+} and Mg^{2+} is calculated to be within 2 % of the total intensity, so that it can be neglected. The operation storage ring was performed at 2.5 GeV of accelerating energy. The ring current was below 200 mA. The flux of incident X-ray was monitored through ionization chamber, which was used for normalization of the profiles. The ranges of S covered were 0.003 to 0.07 $Å^{-1}$ for SAXS and 0.01 to 0.125 $Å^{-1}$ for MAXS, respectively (S is the reciprocal parameter, equal to $2(\sin\theta)/\lambda$, where 2θ is the scattering angle and λ is the wavelength of the X-rays used).

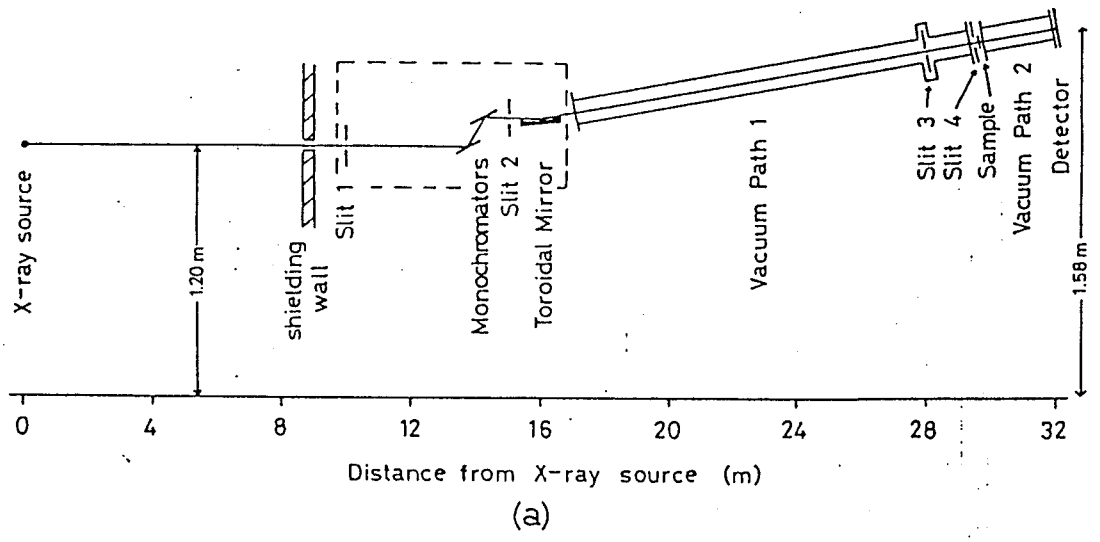

(a)

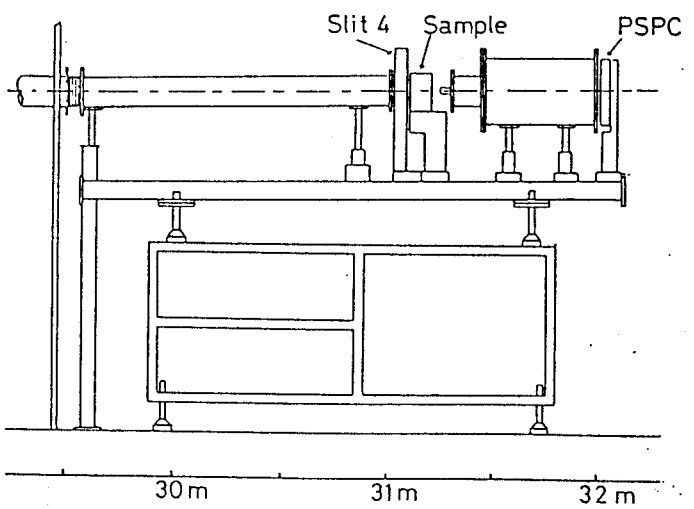

(b)

Figure 6 (a): Schematic drawing of the optics of SAXS apparatus beam line 10C at the PF, Tsukuba, Japan.

Figure 6 (b): Schematic drawing of equipments inside the safety hatch. Figures were taken from Dr. Ueki (43).

The data acquisition of the sample scattering was taken by a PSPC, one-dimensional position sensitive detector (44). The effective length of the detector was 200 mm with a delay line of 400 nS. 2-mm-wide and 6-mm-wide detector apertures were used for SAXS and MAXS, respectively. The signal from the PSPC was converted to time-distance analogue information by CFD, constant-fraction discriminators, then the time difference was converted to digital information of the position by TDC, time to digital converter. The data was stored in MEM, histogram memory and transferred to MINC 11/23 computer (43). The start and stop of collection of data was controlled by the FORTRAN program TST10C.FOR.

The temperature of the sample was maintained at around 5℃. During the exposure, usually 600-1200 sec, the total scattering intensity was monitored. It remained constant, assuring that no aggregation of molecules occurred by the irradiation of X-rays.

6. Data Analysis

The optics is that of quasi-point type so that correction for slit-smearing is unnecessary. Succeeding data treatment was performed only for the profiles whose total scattering was in linear relation with ionization chamber current. Background-corrected SAXS profiles were analyzed using $\ln\{I(S)\}$ *vs.* S^2 (Guinier plot) (45) and $\ln\{I(S)/S\}$ *vs.* S^2 plots (see APPENDIX). For the Guinier analysis, the region of S^2 up to about 1.4×10^{-4} $\mathring{A}^{-2}$ was used. For $\ln\{I(S)/S\}$ *vs.* S^2 analysis, the straight line region of S^2 between 5 and 9×10^{-4} $\mathring{A}^{-2}$ was used. From

the latter, we can estimate the average radius of gyration of two domains, $\overline{Rg}_{N,C}$. Before calculation of distance distribution function, SAXS profile was extrapolated to infinite dilution and was combined with the MAXS profile in S region between 0.02 and 0.06 $\mathring{A}^{-1}$. Distance distribution function was calculated using the indirect transformation method of Glatter (46,47). The maximum length was determined according to the criteria of Glatter. The reproducibility of physical parameters of Tn-C from the analysis was assured by using at least three different preparations of Tn-C.

The computation of SAXS profile and distance distribution function from the atomic coordinates of the Tn-C molecule in crystalline state. The coordinates are available in the Protein Data Bank of Brookhaven National Laboratory, U.S.A. (identification code 4TNC by M.Sundaralingam). The FORTRAN program was written by Mr. Tadasu Shin-i and employs a Monte Carlo procedure for the generation of length distribution function and provides predictions to moderate angle ($\sim 5\mathring{A}$) (48,49). For the results presented here, cubes with an edge length of 5 $\mathring{A}$ and Van der Waals radii taken from Atkins, P.W. (50) were employed.

7. Fundamental Equations of SAXS

The fundamental equations of SAXS profile and other parameters are described below and referenced in (45,51).

Scattering intensity of X-rays (neglect Compton scattering), $I(\vec{S})$, where $\vec{S}$ is reciprocal vector: $|\vec{S}| = \sin 2\theta/\lambda$, λ is the wave length and 2θ is the scattering angle, can be written as

follows:

$$I(\vec{S}) = F(\vec{S})F^*(\vec{S}) \qquad (1)$$

$$F(\vec{S}) = \int_v \rho(\vec{r})\exp(2\pi i\vec{S}\vec{r})\, d\vec{r}$$

$\rho(\vec{r})$: excess scattering density at $\vec{r}$

F^* : conjugate complex of F

In small angle scattering, particles can take any orientation with equal probability. Then, the spatial average of $\exp(2\pi i\vec{S}\vec{r})$ is equal to $\sin(2\pi Sr)/(2\pi Sr)$ and $I(\vec{S})$ yields the isotropic intensity function, I(S).

$$I(S) = \int_v\int \rho(\vec{r}_1)\rho(\vec{r}_2)\sin(2\pi Sr)/(2\pi Sr)d\vec{r}_1\, d\vec{r}_2 . \qquad (2)$$

where $r = |\vec{r}_1 - \vec{r}_2|$.

This integral can be extended by writing

$$I(S) = \int\{\rho(\vec{r}_1)\int_0^\infty\int_0^{4\pi}\rho(\vec{r}_1+\vec{r})\sin(2\pi Sr)/(2\pi Sr)r^2 d\omega dr\}d\vec{r}_1$$

The partial integral can be defined as

$$4\pi\,\gamma(r) = \int_0^{4\pi}\{\int \rho(\vec{r}_1)\rho(\vec{r}+\vec{r}_1)d\vec{r}_1\}d\omega$$

$$= 4\pi\,\langle\rho(\vec{r})*\rho(-\vec{r})\rangle.$$

Then

$$I(S) = 4\pi\int_0^\infty\gamma(r)\sin(2\pi Sr)/(2\pi Sr)r^2dr$$

$$= \int_0^\infty P(r)\sin(2\pi Sr)/(2\pi Sr)dr \qquad (3)$$

where

$$P(r) = 4\pi r^2\,\gamma(r). \qquad (4)$$

The inverse fourier transform gives

$$P(r) = 8\pi r \int_0^\infty SI(S)\sin(2\pi Sr)dS. \qquad (5)$$

From the above definition, the P(r) function obtained by sine transform of the intensity function represents the distance distribution function inside the particle.

An important physical parameter, obtainable from the SAXS profile, is the radius of gyration, Rg. At small value of S, the Taylor expansion series gives

$$\sin(2\pi rS)/(2\pi rS) = 1-(2\pi rS)^{2}/3$$
$$= \exp\{-(2\pi rS)^{2}/3\}$$

So

$$I(S) = I(0)\exp\{-(4\pi^{2}/3)\,Rg^{2}S^{2}\} \qquad (6)$$

where

$$I(0) = \int_V\int \rho(\vec{r}_1)\rho(\vec{r}_2)d\vec{r}_1\,d\vec{r}_2\,, \qquad (7)$$

$$Rg^2 = \frac{\int_V\int \rho(\vec{r}_1)\rho(\vec{r}_2)|\vec{r}_1-\vec{r}_2|^2\,d\vec{r}_1\,d\vec{r}_2}{2\int_V\int \rho(\vec{r}_1)\rho(\vec{r}_2)d\vec{r}_1\,d\vec{r}_2}$$
$$= \frac{\int_V \rho(\vec{r})r^{2}d\vec{r}}{\int_V \rho(\vec{r})\,d\vec{r}}\,. \qquad (8)$$

The logarithm of Eq.(6) gives,

$$\ln(I(S)) = \ln(I(0))-4\pi^{2}/3\,Rg^{2}\,S^{2} \qquad (9)$$

This equation shows that a linear region always exists at small S in $\ln\{I(S)\}$ <u>vs.</u> S^2 plot (Guinier plot) and that its tangent offers an important structural parameter.

We developed the SAXS equations for a dumbbell-shaped object in minimum assumption and obtained additional structural parameters; average radius of gyration of each domain ($\overline{Rg}_{N,C}$ and the distance between two domains (r_{NC}) (36). The detail of the analysis was described in APPENDIX. The following equation is valid near $S = 1/r_{NC}$ for I(S) of dumbbell-shaped object as,

$$\ln\{I(S)/S\} = \ln\{2n(dom)^2 r_{NC}\} - (4\pi^2/3)\overline{Rg}_{N,C}^2 S^2. \qquad (A\text{-}10)$$

Eq (10) indicates that the $\ln\{I(S)/S\}$ *vs.* S^2 plot must have a linear region around $S = 1/r_{NC}$, and that the slope of the straight line in the plot yields $\overline{Rg}_{N,C}$. Since the Rg of the molecule was described as

$$Rg^2 = \overline{Rg}_{N,C}^2 + r_{NC}^2/4 \qquad (A\text{-}7)$$

r_{NC} can be estimated from Rg and $\overline{Rg}_{N,C}$ of the molecule.

Above SAXS equations requires the assumption that scattering particles take all orientation with equal probability and that there is no long-range order. The observed scattering intensity is however expressed as a function of the intrinsic scattering intensity of an particle as well as of the statistical function governing their arrangement. The structural parameters from the inner part of SAXS profiles such as Rg and I(0) therefore depends on protein concentration, *i.e.*, concentration effect. The relation between statistical function governing the arrangement and the forward scattering intensity, I(0)/C was derived by Eisenberg (52). I(0)/C is expressed as a fluctuation of electron density and can be

represented in another form (52),

$$I(0)/C = \frac{(\partial \rho / \partial C)^2}{1/M + 2AC + 3BC^2} \qquad (10)$$

where M is a molecular weight, A and B are virial coefficient. This formula is identical to the Zimm equation in light scattering. Normally the second virial coefficient is positive by the exclusion volume effect so that Eq (10) theoretically supports the linear relationship between protein concentration and I(0)/C. Rg dependence on protein concentration is also explained by this equation. The Rg's and I(0)/C's dependence on protein concentration becomes larger as the asymmetry of the molecule increases since the second virial coefficient becomes smaller.

When I(0)/C is extrapolated to infinitely dilute solution, I(0)/C becomes proportional to molecular weight as in (51)

$$I(0)/C \propto M(\Delta z)^2 \qquad (11)$$

where Δz, the electron density difference (electron mol/g protein), is $(z-\nu d)$, where z is the electron density of the protein; ν is the partial specific volume of the protein(ml/g); and d is the electron density of the solvent (electron mol/ml). Making use of this formula, we can obtain the molecular weight of the molecule from the absolute intensity of forward scattering (51). Not knowing its absolute value, it is possible to estimate the molecular weight of the molecule by comparing the relative intensity of I(0)/C with that of a protein whose molecular weight is known, provided that the two proteins have

the same Δz (41). In the present study, lysozyme was used for the reference protein.

When the sample is not monodisperse, i.e., contaminated with dimer, apparent I(0)/C is expressed as (45),

$$I(0)/C = \frac{N_m}{N_m + 2N_d} I_m(0)/C + \frac{N_d}{N_m + 2N_d} I_d(0)/C$$

where $I_m(0)$ and $I_d(0)$ are forward scattering of monomer and dimer, respectively; N_m and N_d are molar concentration of monomer and dimer, respectively. Since $I_d(0)$ equals to $4I_m(0)$, above equation becomes

$$I(0)/C = \frac{N_m + 4\ N_d}{N_m + 2\ N_d} I_m(0)/C \qquad (12)$$

Apparent Rg is expressed as,

$$Rg^2 = \frac{N_m\ Rg_m^2 + 4N_d\ Rg_d^2}{N_m + 4N_d} \qquad (13)$$

where Rg_m and Rg_d are Rg of monomer and dimer, respectively. Eqs. (12) and (13) do not take account for concentration effect. Since fraction of dimer increases with increasing total concentration, apparent I(0) and Rg are supposed to increase.

RESULTS

1. General Features of SOXS Profiles from Tn-C

Figure 7 shows SAXS profiles, I(S)'s, from Tn-C solution (above 20 mg/ml protein) with different amount of Ca^{2+} and Mg^{2+}. The ordinate for each ln{I(S)} is shifted so as to demonstrate the profile clearly. All scattering profiles in the very small-angle region suffered very much from the effect of high protein concentration, i.e., a downward curvature in these plots at very small angles (53). The inner part of the profiles were extrapolated to infinte dilution. This concentration effect of Tn-C is apparently related to the surface property of Tn-C around neutral pH (see Eq [10]). The profiles at higher scattering angles are not affected by the protein concentration effect: they remain unchanged for solutions with decreasing concentration. This behavior seems to be somewhat different from SAXS observation on water-soluble proteins with molecular mass less than 20,000 daltons. The SAXS profiles from myoglobin and lysozyme solutions do not show such an effect even at a concentration of about 50 mg/ml. Calmodulin, another Ca^{2+} binding dumbbell-structured protein, however shows similar characteristics in the profiles (54).

Another characteristic feature of these profiles is a "hump", which is characteristic of the dumbbell structure. This "hump" appears at about S = 0.027 $\mathring{A}^{-1}$ and is shown by the arrows. The "hump" does not appear in scattering profiles of tryptic fragments of Tn-C irrespective of Ca^{2+}.

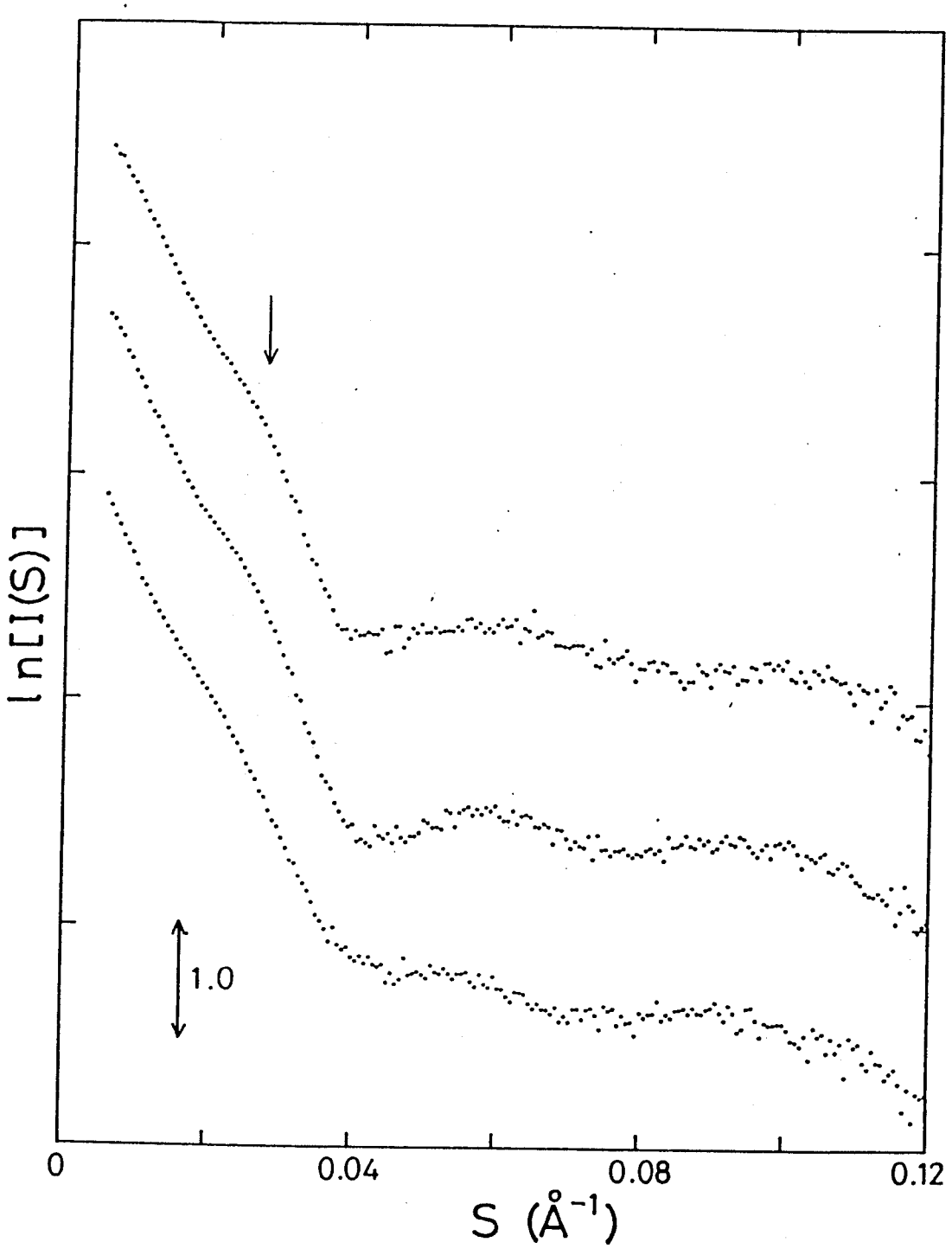

Figure 7 (a): SOXS profiles from Tn-C in the absence of Mg^{2+}. The inner part of SOXS profiles were extrapolated to infinitely diluted solution. From bottom Ca_0Tn-C and Ca_2Tn-C and Ca_4Tn-C.

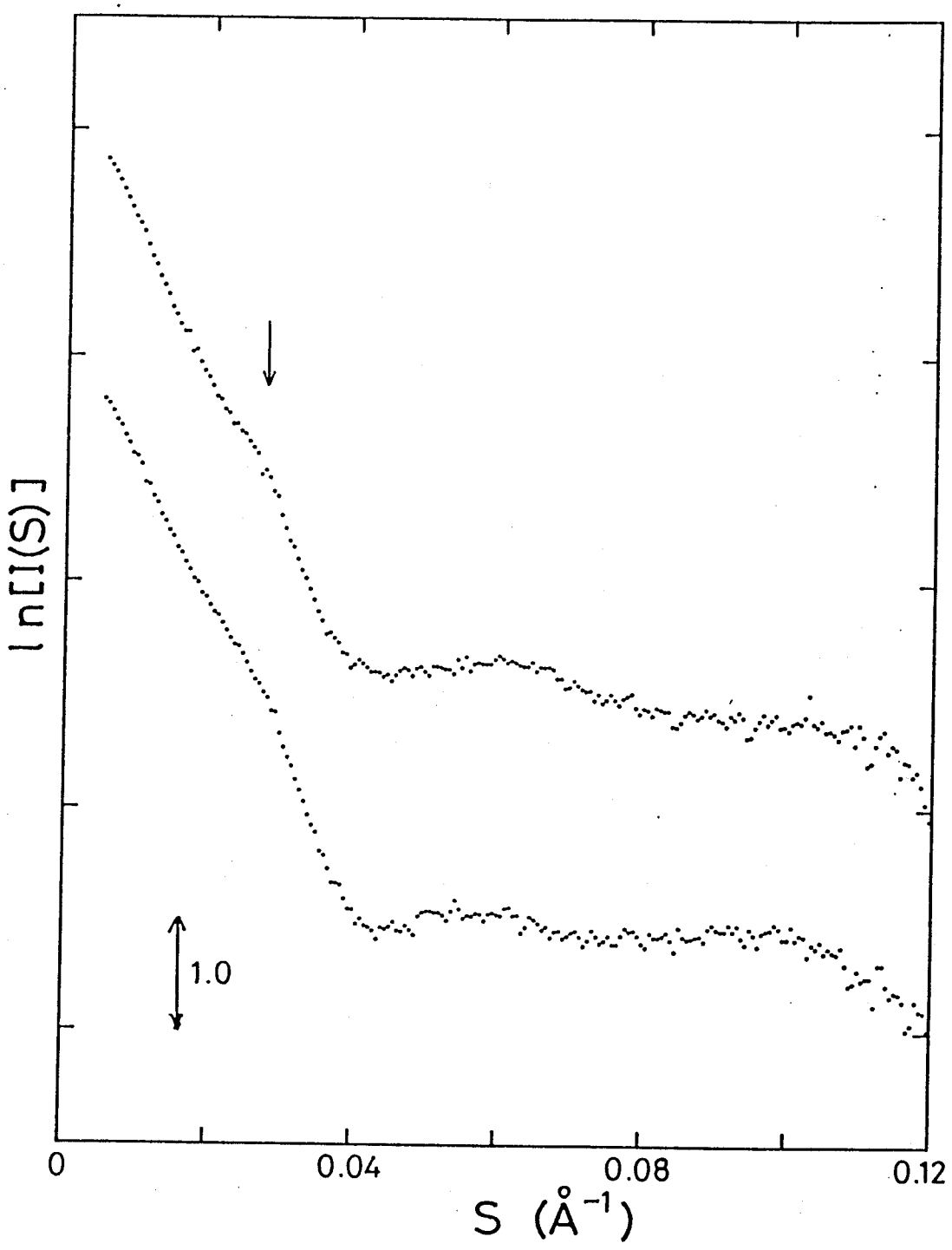

Figure 7 (b): SOXS profiles from Tn-C in the presence of Mg^{2+}. The inner part of SOXS profiles were also extrapolated to infinitely diluted solution. From bottom Mg_2Ca_0Tn-C and Mg_2Ca_2Tn-C.

2. Structural Change of Tn-C upon Ca^{2+} Binding in the Absence of Mg^{2+}

2.a. Radius of Gyration of Tn-C

Figure 8 shows good linearity for the inner part of SAXS profiles from Tn-C in Guinier plot in three different states of Ca^{2+} binding. Upward curvature is not seen in these plots and hence no apparent aggregation is detected.

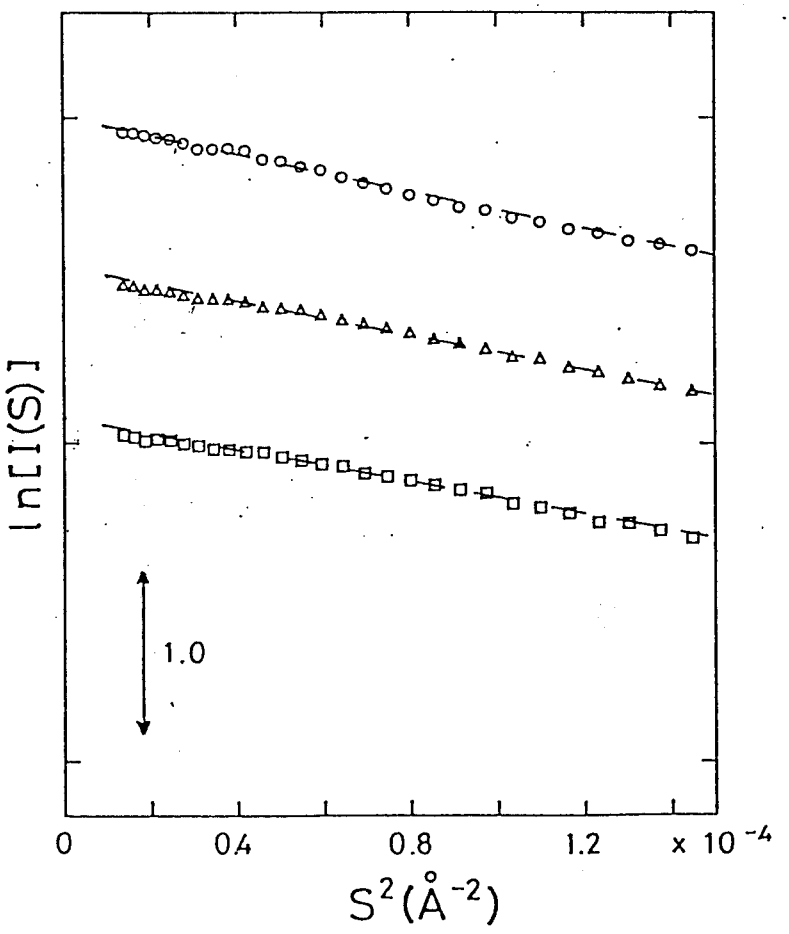

Figure 8: The Guinier plots, ln[I(S)] *vs.* S^2, of SAXS profiles from Tn-C solutions that contain different amounts of Ca^{2+}: Ca_0Tn-C (○), Ca_2Tn-C (△), and Ca_4Tn-C (□). The sample buffer is 0.1 M KCl, 2 mM EDTA, and 10 mM MOPSO/KOH (pH 7.0). The concentration of Tn-C was 10 mg/ml.

The effect of protein concentration on scattering intensity is shown in Figure 9 for Ca_0Tn-C. It evidently shows a pronounced concentration effect of Tn-C, that is a linear decrease of intensity at small angles with increasing protein concentration. The profiles exhibit an identical curvature at larger S, $S \geqq 0.01$ $\mathring{A}^{-1}$. Such an effect was also observed both for Ca_0Tn-C and Ca_4Tn-C but becomes less notable when increasingly bound to Ca^{2+}. Each scattering profile was extrapolated to an infinite dilution in the Zimm plot for the purpose of elimination of interparticle interference. Rg obtained by Guinier plot depends on protein concentration. Figure 10 shows the dependence of Rg's on the protein concentration. By linear extrapolation of Rg's to infinite dilution, the Rg's of Tn-C in the absence of Mg^{2+} were found to be 27.8 ± 0.3 Å, 23.8 ± 0.2 Å and 22.6 ± 0.1 Å for Ca_0Tn-C, Ca_2Tn-C and Ca_4Tn-C, respectively. These values do not deviate from Rg's obtained by linear extrapolation of Rg^2 to infinitely dilute solution (55). Rg of the molecule decreases remarkably in Ca^{2+} occupation to high affinity sites, while the change is not so appreciable for the change in Ca^{2+} occupation to low affinity sites. Forward scattering, I(0)/C obtained from Guinier plots is plotted for protein concentration in Figure 11. Both Figures 10 and 11 exhibit a considerable liner decrease with increasing protein concentration. These plots suggest that the aggregation of Tn-C does not occur within the employed concentration range, 2-10 mg/ml.

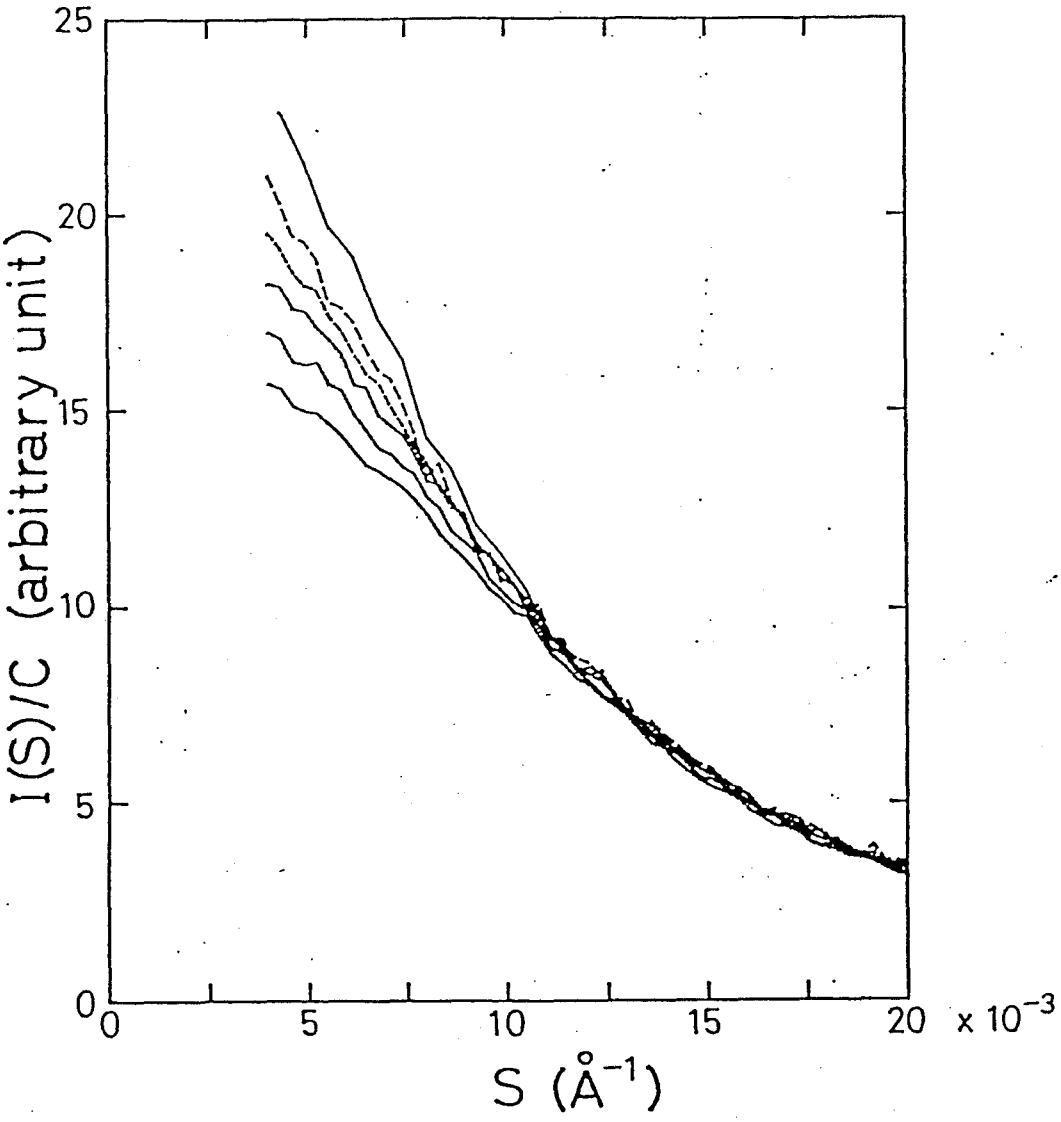

Figure 9: SAXS profiles of Ca_0Tn-C. From the bottom different concentrations of the protein concentrations are 10, 8, 6, 4, and 2 mg/ml, respectively. Note that the scattering curve, I(S)/C, decreases with increasing protein concentration. The solid line (top) is the scattering profile extrapolated to zero protein concentration. The curves are normalized to C = 1 (mg/ml).

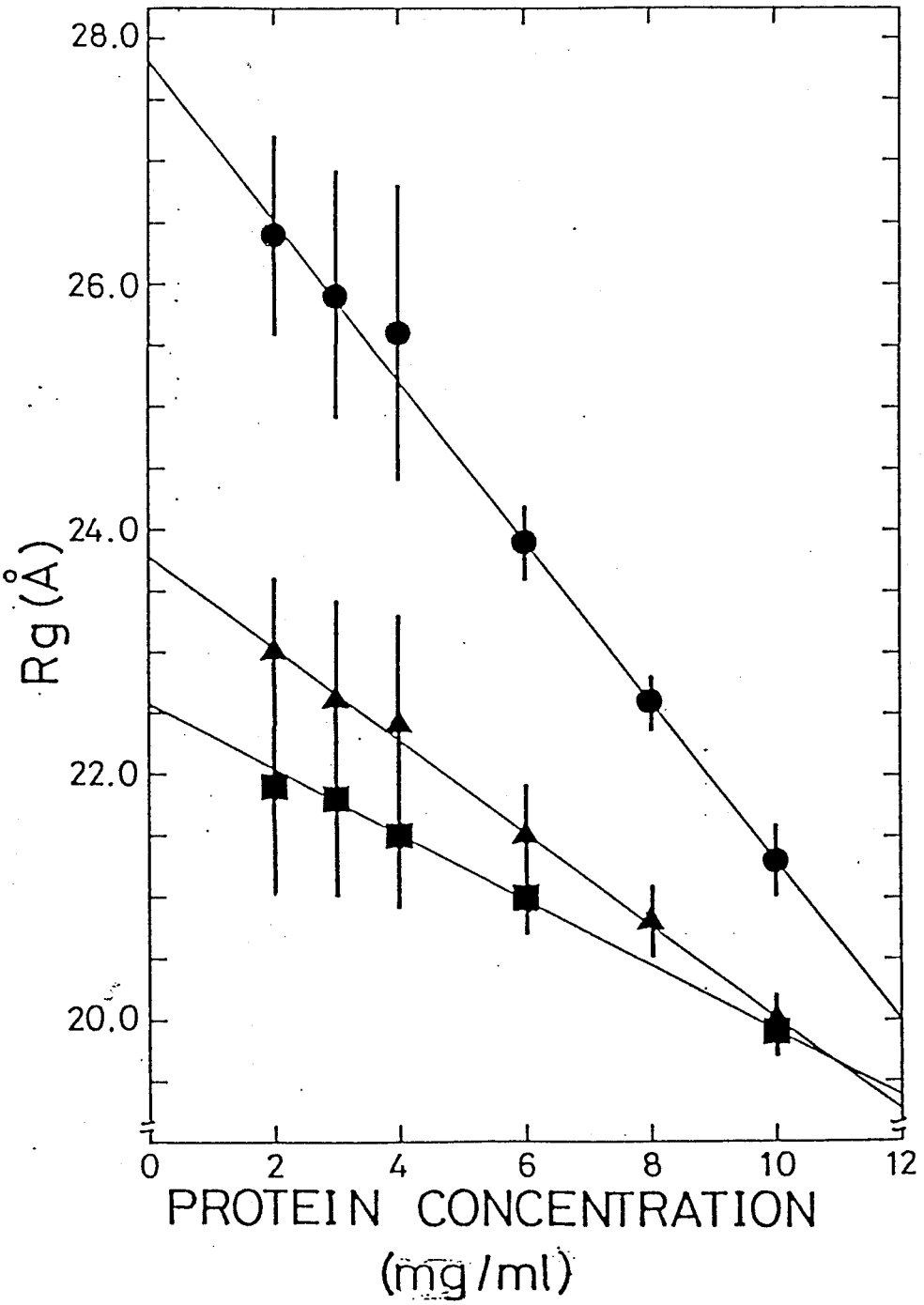

Figure 10: Protein concentration dependence of the apparent radii of gyration of Ca_0Tn-C (●), Ca_2Tn-C (▲), and Ca_4Tn-C (■). The large S.D. of Rg's in dilute concentrations (less than 4 mg/ml) include the deviation of different samples.

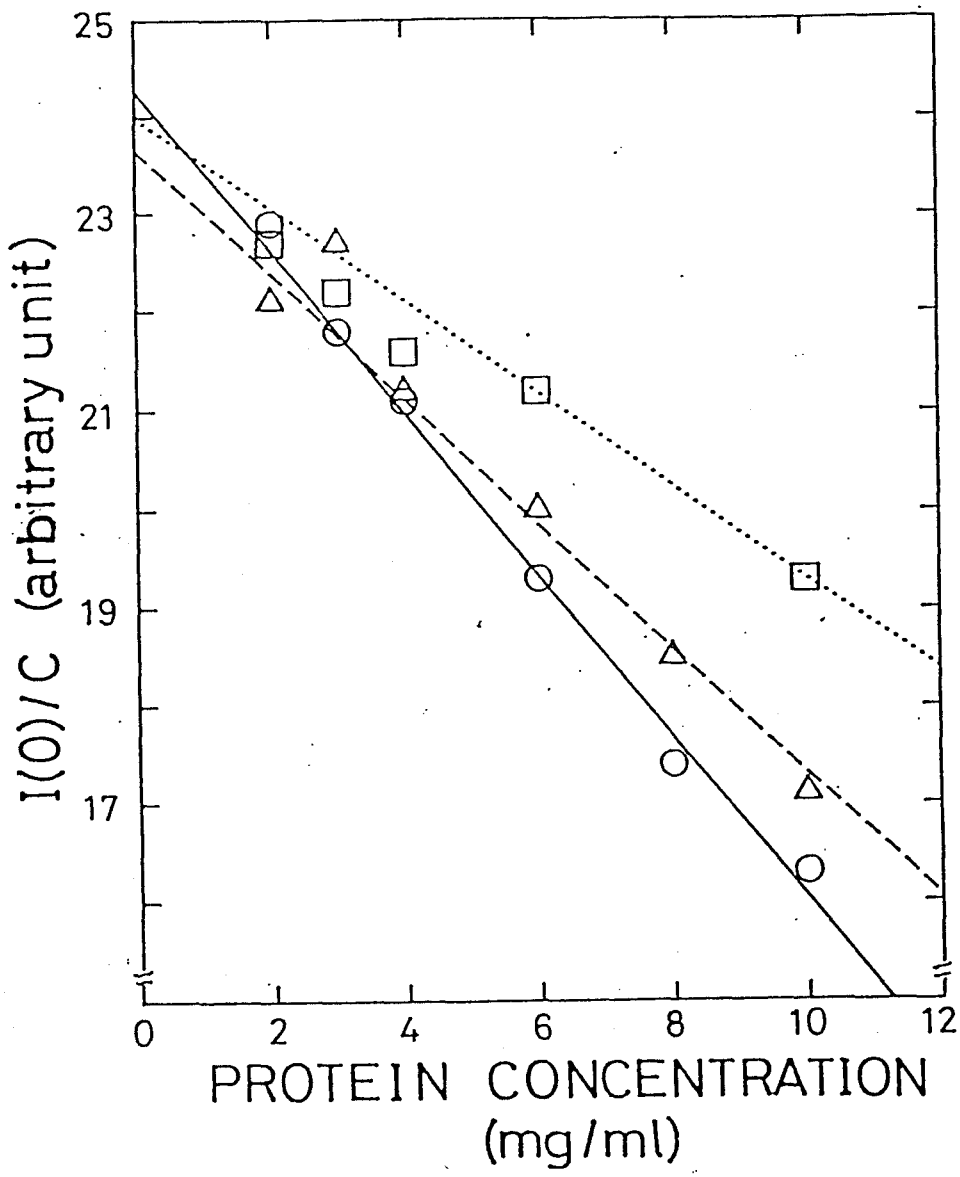

Figure 11: Protein concentration dependence of forward scattering, I(0)/C, obtained from the Guinier plot approximation for Ca_0Tn-C (○), Ca_2Tn-C (△), and Ca_4Tn-C (□). As in Figure 10, a linear decrease of I(0)/C with increasing protein concentration is evident.

2.b. Molecular Weight Determination

On the basis of Eq (10) the molecular weights were estimated from I(0)/C's of Tn-C and lysozyme at infinite dilution and found to be 22,300 ± 550, 21.800 ± 400, and 22,000 ± 700 for Ca_0Tn-C, Ca_2Tn-C and Ca_4Tn-C, respectively. These values are larger than the molecular weight determined by amino acid sequence, 17,846 but identical with Murray & Kay's results (16). No apparent aggregation was observed upon Ca^{2+} binding to Tn-C. Presumably the difference between 18,000 and 22,000 is attributed to the difference of Δz between Tn-C and lysozyme.

2.c. Distance Distribution Function

As described earlier the distance distribution function, P(r) shows the frequency of the interatomic vector of a given length in a molecule. In Figure 12, P(r) of Tn-C has two maxima, one distinct and the other as a shoulder, and these maxima are characteristic of a "dumbbell"-shaped object as described by Seaton *et al.* (54), Heidorn & Trewhella and Hubbard *et al.* (30,31). This feature was also reported for calmodulin, whose structure in crystal is known to be a dumbbell structure. This supports the idea that irrespective of Ca^{2+} Tn-C keeps dumbbell shape in solution as well as in crystalline state. For the dumbbell structure, the first maximum peak appears near the value of the radius of each domain and the second maximum at about r_{NC} is from the correlation of two domains. As for Ca_0Tn-C the first peak is rather broad, centered at 22 Å. When Ca^{2+} ions bind to C-domain, it becomes sharper and its center shifts to a

smaller value by about 2 Å. This is again consistent with the decrease in $\overline{Rg}_{N,C}$. The position of the second peak shifts to a smaller value with increasing Ca^{2+}, which also indicates the shortening of interdomain distance, r_{NC}. The decrease of P(r) in r = 60-80 Å region by adding Ca^{2+} implies that the electron density shifted to the center of Tn-C molecule upon Ca^{2+} binding.

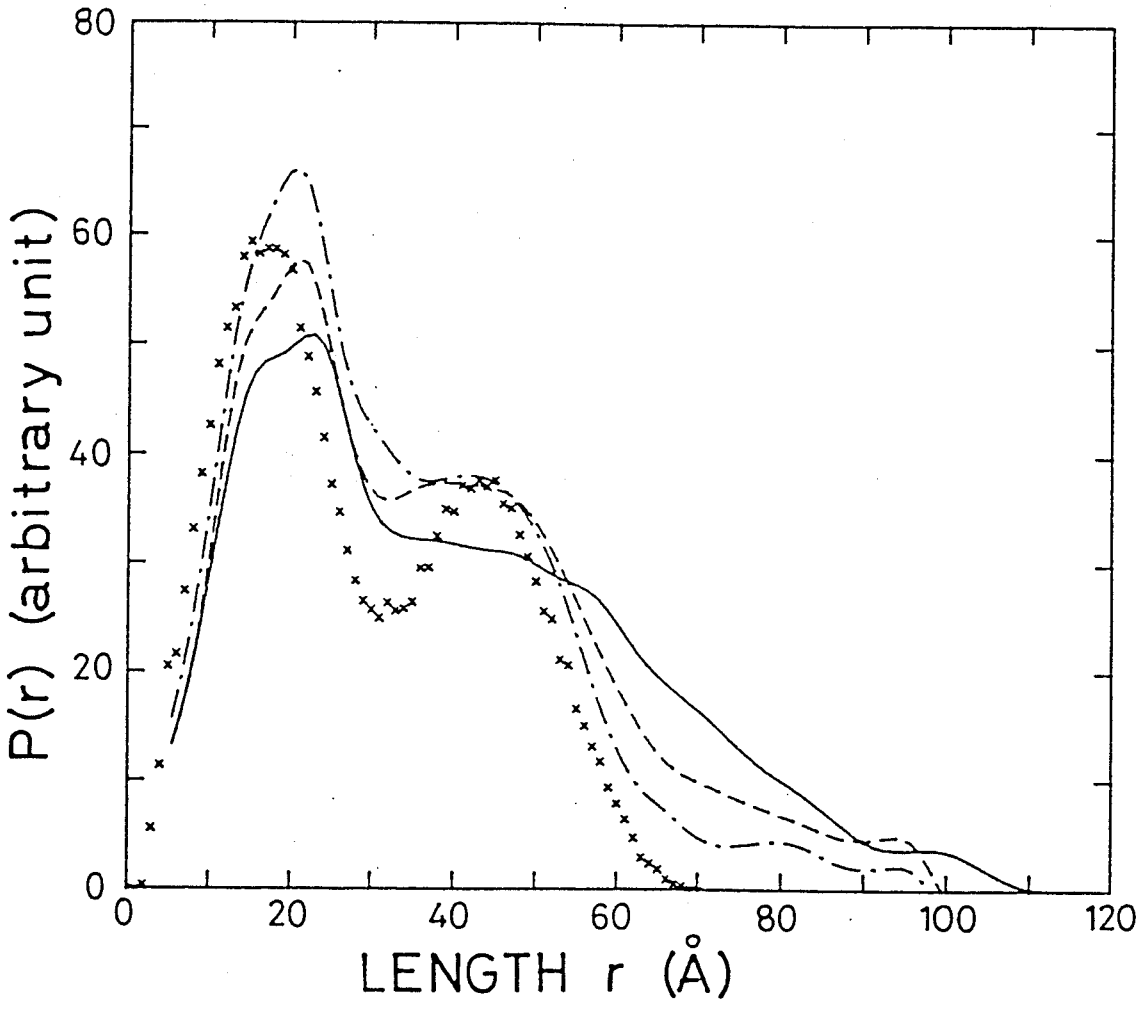

Figure 12: The distance distribution function, P(r), at pH 7.0 for Ca_0Tn-C (solid line), Ca_2Tn-C (broken) and Ca_4Tn-C (chain-dotted line). The P(r) function of Tn-C in the crystalline state (x) was calculated with atomic coordinates, cited from the Brookhaven Protein Data Bank, available in the Institute for Protein Research, Osaka University.

2.d. SAXS Analysis Based on Dumbbell Structure

Both the SAXS profile and P(r) of Tn-C is well explained by a dumbbell-shaped model. With this model, two physical parameters, i.e., the average radius of domains ($\overline{Rg}_{N,C}$) and distance between the two centers of domain (r_{NC}), can be estimated (see APPENDIX). $\overline{Rg}_{N,C}$'s were calculated from the slope in ln{I(S)/S} vs. S^2 plot (in Figure 13). Together with Rg and $\overline{Rg}_{N,C}$ the r_{NC} can be calculated by Eq. A-7 in APPENDIX. These values are listed in Table 3.

Table 3 : Structural parameters of Tn-C in the absence of Mg^{2+} from the analysis of the intrinsic profile

	Ca_0Tn-C	Ca_2Tn-C	Ca_4Tn-C
Rg	27.8 ± 0.3 Å	23.8 ± 0.2 Å	22.6 ± 0.1 Å
$\overline{Rg}_{N,C}$	15.4 ± 0.3 Å	14.8 ± 0.2 Å	14.6 ± 0.1 Å
r_{NC}	46.3 ± 1.0 Å	37.3 ± 0.8 Å	34.5 ± 0.4 Å
MW	22,300 ± 600	21,800 ± 400	22,000 ± 600

Occupation of high affinity sites by Ca^{2+} decreases $\overline{Rg}_{N,C}$ by 4 %. The decrease in $\overline{Rg}_{N,C}$ of this stage accounts for 75 % of the total change. This means that the Ca^{2+} binding to the high affinity sites induces a tightening of C-domain and is consistent with the increase in α-helix content. On the other hand, Ca^{2+} binding to low affinity sites seems to not bring about an appreciable conformational change in N-domain since $\overline{Rg}_{N,C}$

decreases only by a slight amount. r_{NC} decreases from 46 Å to 37 Å with increasing Ca^{2+} concentration.

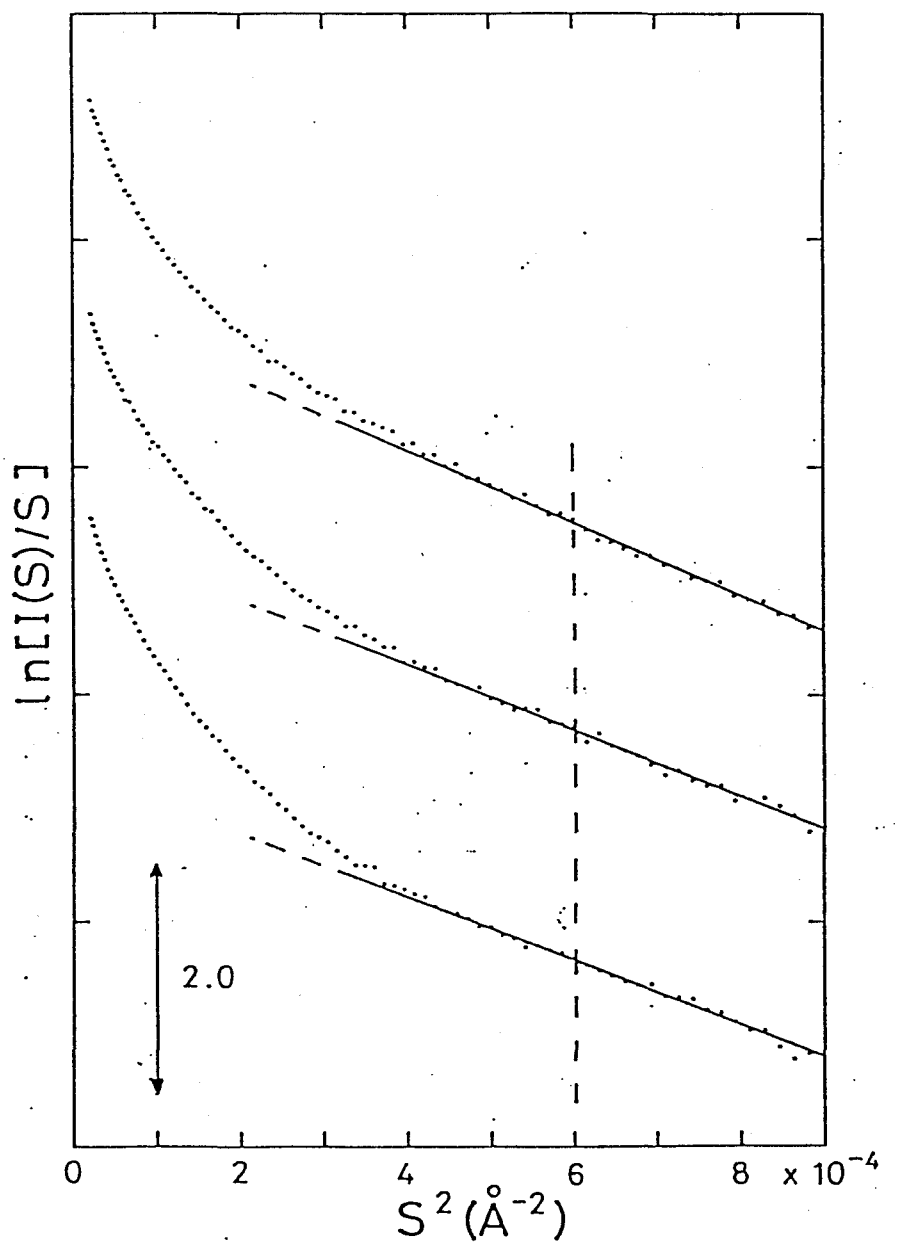

Figure 13: The ln[I(S)/S] *vs.* S^2 plots for the scattering profiles from Tn-C solutions. $\overline{Rg}_{N,C}$ is derived from the slope in the linear region around $S^2 = 6 \times 10^{-4}$ Å^{-2}. From bottom Ca_4Tn-C, Ca_2Tn-C and Ca_0Tn-C.

3. Structural Change of Tn-C upon Ca^{2+} Binding in the Presence of Mg^{2+}

3.a. Radius of Gyration of Tn-C

Figure 14 shows good linearity for the inner part of SAXS profiles in Guinier plot for Mg_2Ca_0Tn-C and Mg_2Ca_2Tn-C. It is the same as in the case of Mg^{2+}-free experiments.

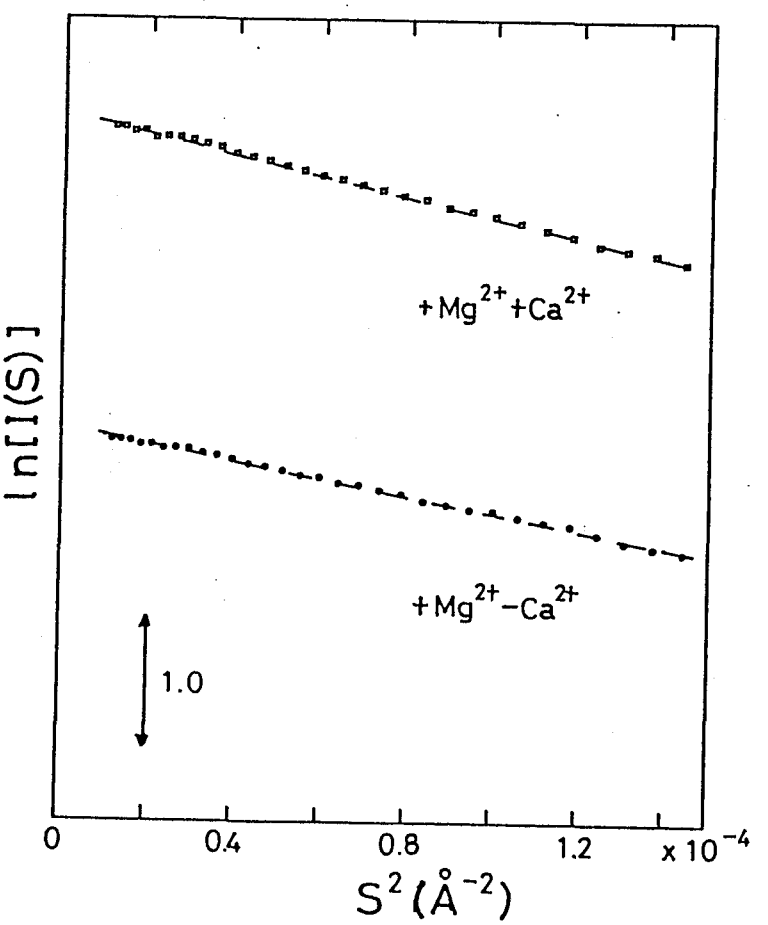

Figure 14: The Guinier plots, ln[I(S)] *vs.* S^2 of SAXS profiles from Tn-C solutions that contain different amounts of Ca^{2+} in the presence of Mg^{2+}; Mg_2Ca_0Tn-C (○) and Mg_2Ca_2Tn-C (□). The sample buffer was 0.1 M KCl, 2mM EGTA, 2 mM $MgCl_2$, and 10 mM MOPSO//KOH(pH 7.0). The concentration of Tn-C was 8 mg/ml.

The large effect of protein concentration on scattering intensity was also observed for Mg_2Ca_0Tn-C (Figure 15 (a)). SAXS profile of Mg_2Ca_2Tn-C, whereas, has less pronounced effect (Figure 15 (b)). Especially, I(S)/C of Mg_2Ca_2Tn-C increases with increasing protein concentration, which is indicative of existence of aggregation.

Rg's obtained by the Guinier plot for Mg_2Ca_0Tn-C and Mg_2Ca_2Tn-C were plotted in Figure 16. A good linearity of Rg's was observed for both Mg_2Ca_0Tn-C and Mg_2Ca_2Tn-C. The dependency of Rg's of Mg_2Ca_2Tn-C on protein concentration was in sharp contrast with that of I(S)/C: if dimerization occurs, it is natural for Rg's of Mg_2Ca_2Tn-C to increase with increasing protein concentration, whereas, Rg's decrease. By linear extrapolation of Rg's to infinite dilution, the Rg's of Tn-C were found to be 24.3 ± 0.2 Å and 25.1 ± 0.1 Å for Mg_2Ca_0Tn-C and Mg_2Ca_2Tn-C, respectively. A linear extrapolation of Rg^2 also yielded similar data.

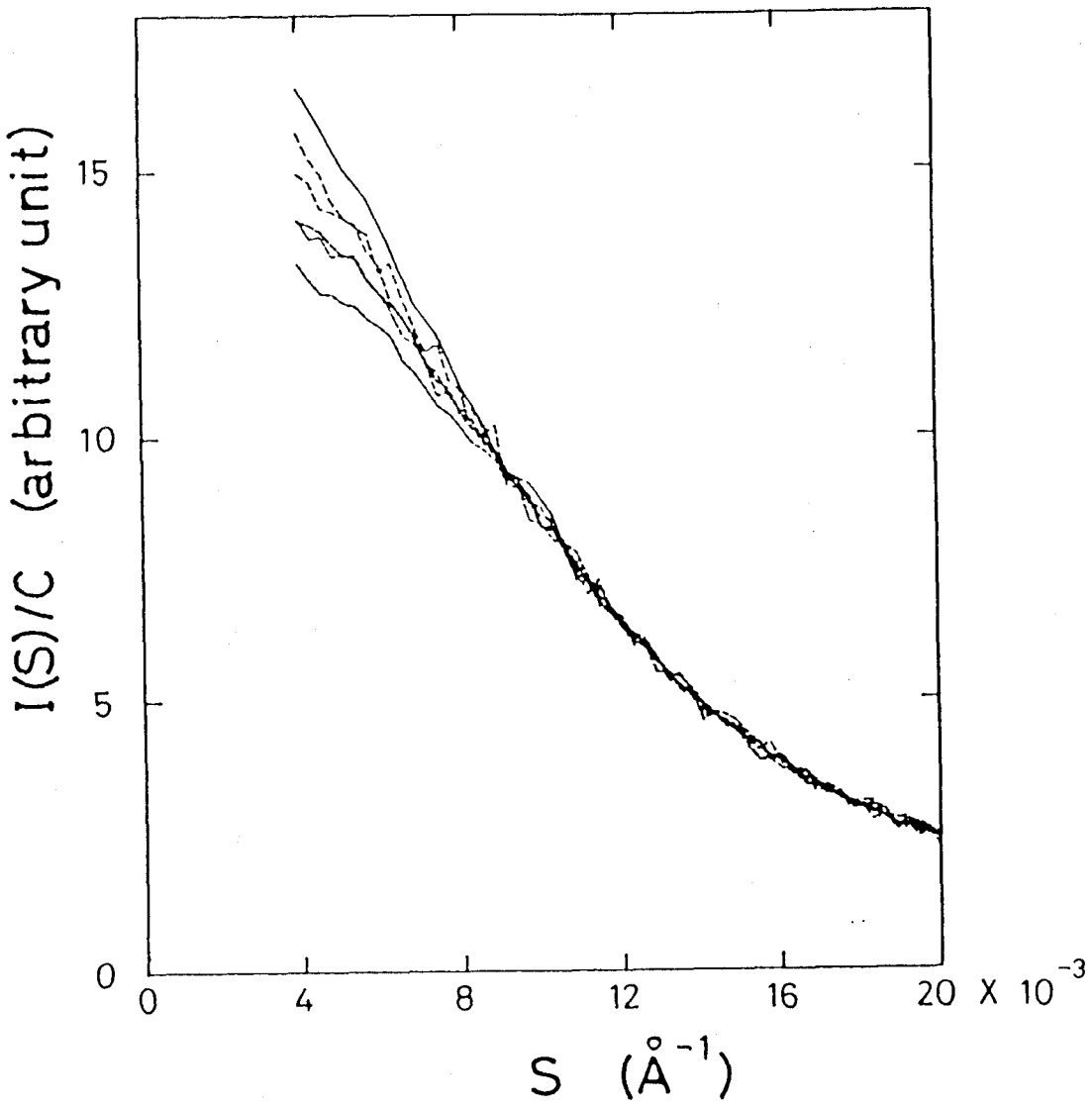

Figure 15 (a): SAXS profiles of Mg_2Ca_0Tn-C. From the bottom different concentrations of the protein concentrations are 10, 8, 6, 4, and 2 mg/ml, respectively. Note that the scattering curve, I(S)/C, decreases with increasing protein concentration, which is the same as in Figure 9. The solid line (top) is the scattering profile extrapolated to zero protein concentration. The curves are normalized to C = 1 (mg/ml).

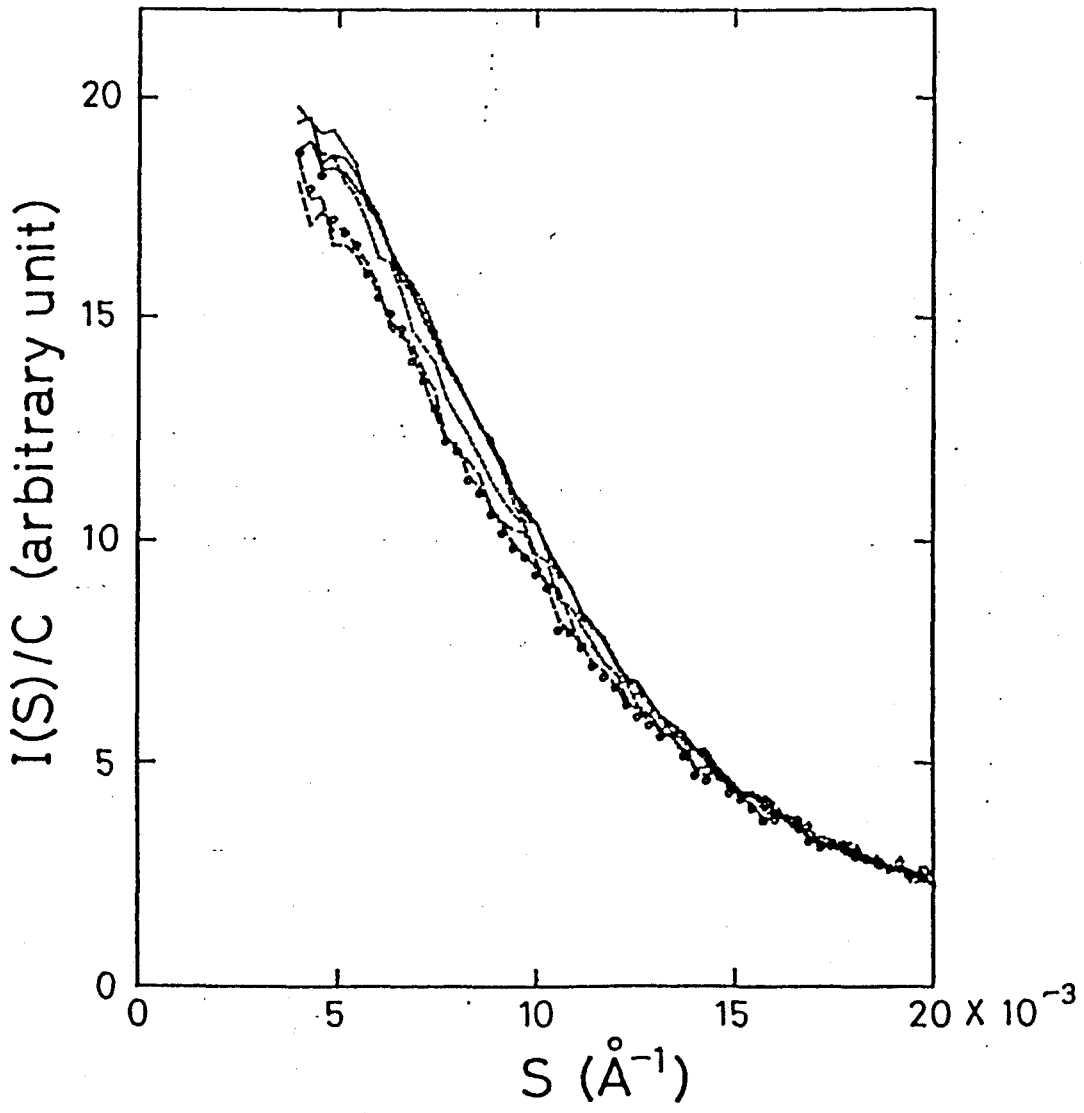

Figure 15 (b): SAXS profiles of Mg_2Ca_2Tn-C. From the bottom different concentrations of the protein concentrations are 2, 4, 6, 8 and 10 mg/ml, respectively. Note that the scattering curve, I(S)/C, increases with increasing protein in 2-6 mg/ml, while at 6, 8, 10 mg/ml I(S)/C remains unchanged. The solid line (top) is the scattering profile extrapolated to zero protein concentration. The curves are normalized to C = 1 (mg/ml).

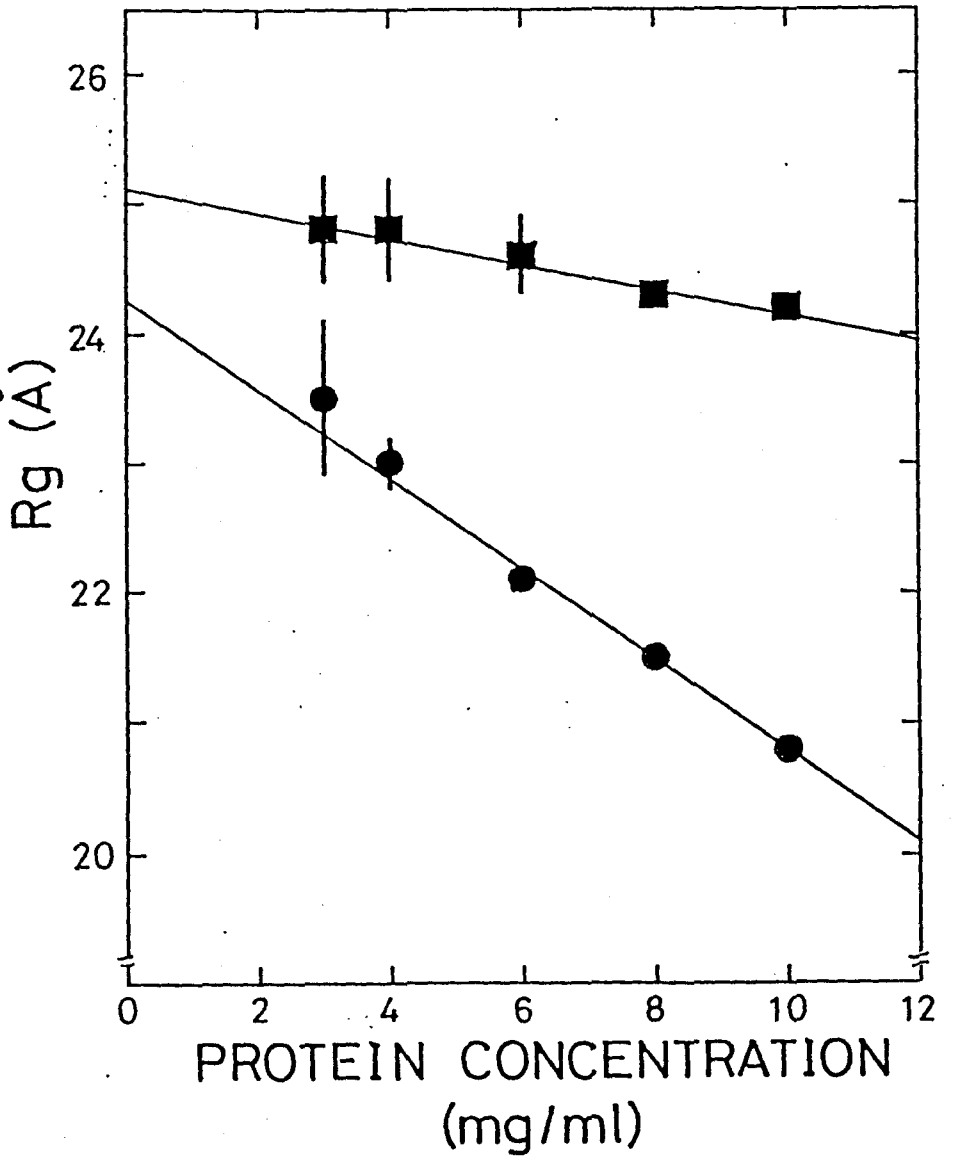

Figure 16: Protein concentration dependence of the apparent radii of gyration of Mg_2Ca_0Tn-C (●), Mg_2Ca_2Tn-C (■). The error bars represent one σ of the data.

3.b. Molecular Weight Determination

The molecular weight of Mg_2Ca_0Tn-C was also estimated by the same method described previously. The dependency of I(0)/C on protein concentration was shown in Figure 17. A good linearity of I(0)/C with increasing protein concentration was observed in Mg_2Ca_0Tn-C, and was also seen in the absence of Mg^{2+} (Figure 16). Considering the good linearity in Figures 16 and 17, Mg_2Ca_0Tn-C does not aggregate. Its molecular weight was 21,600 ± 500 and is the same value as Tn-C's in the absence of Mg^{2+}. On the other hand, I(0)/C of Mg_2Ca_2Tn-C behaves in a more complicated manner: I(0)/C increases in the region of 2-6 mg/ml while in 6-10 mg/ml I(0)/C decreases with increasing protein concentration, which is indicative of the existence of dimer.

3.c. Distance Distribution Function

P(r)'s obtained from extrapolated SOXS profiles are plotted in Figure 18. Since SAXS profiles were extrapolated to infinite dilution, P(r) of Mg_2Ca_2Tn-C calculated from it sufficiently exhibits the intrinsic P(r). The characteristic of dumbbell-shaped object was also observed in the same way as Mg^{2+}-free Tn-C. Especially P(r) of Mg_2Ca_0Tn-C resembles that of Ca_2Tn-C.

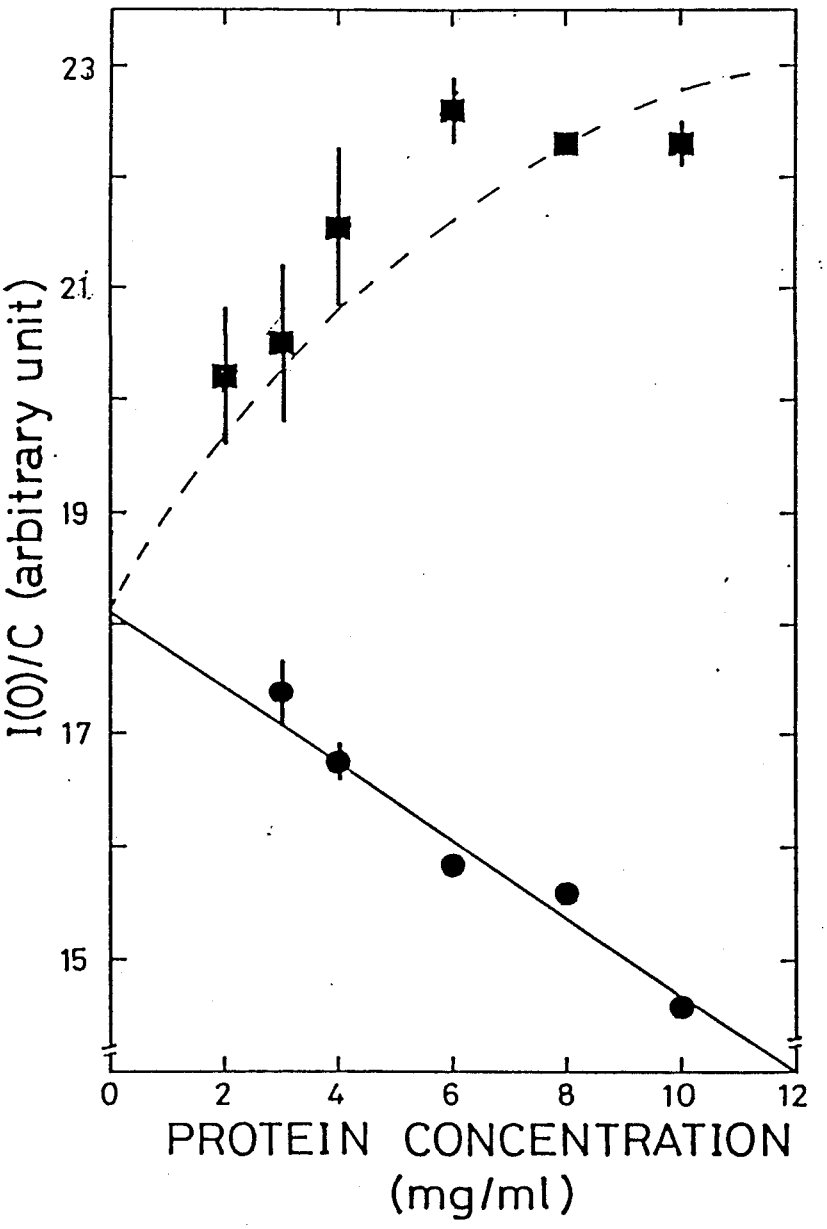

Figure 17: Protein concentration dependence of forward scattering, I(0)/C, obtained from the Guinier plot approximation for Mg_2Ca_0Tn-C and Mg_2Ca_2Tn-C. As in Figure 11, a linear decrease of I(0)/C for Mg_2Ca_0Tn-C with increasing protein concentration is evident. Mg_2Ca_2Tn-C however increases. Broken line was calculated assuming monomer-dimer equilibrium with apparent dimerization constant K = 511 M^{-1}.

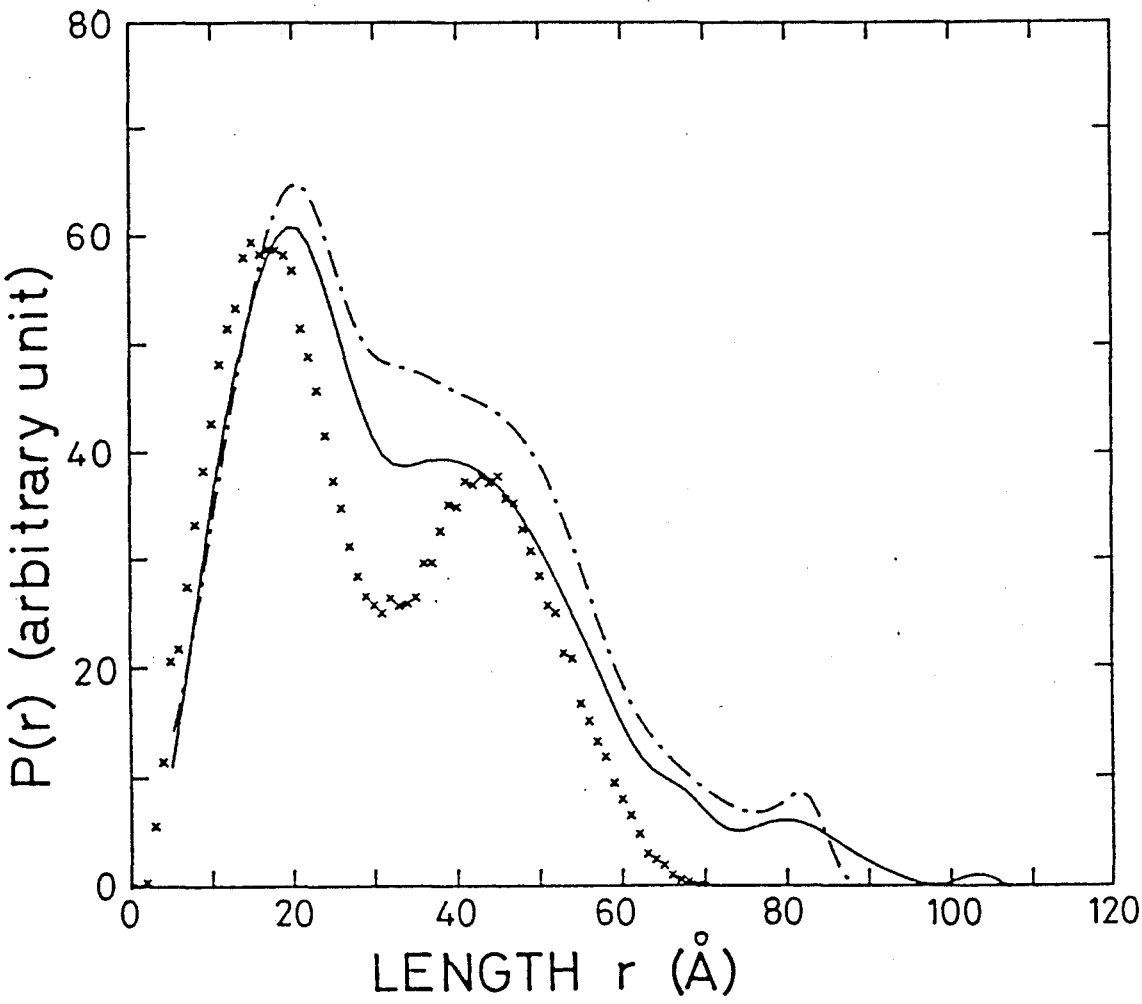

Figure 18: Distance distribution function, P(r) of Mg_2Ca_0Tn-C and Mg_2Ca_2Tn-C from extrapolated SOXS profiles: Mg_2Ca_0Tn-C (solid line), Mg_2Ca_2Tn-C (chain-dotted line) and crystal structure (x).

3.d. SAXS Analysis Based on Dumbbell Structure

Since the major characteristics of X-ray scattering from Tn-C are common to Tn-C irrespective of the presence of Mg^{2+}, $\overline{Rg}_{N,C}$ and r_{NC} were also obtained by the same method as Mg^{2+}-free Tn-C. $\overline{Rg}_{N,C}$ was 15.1 ± 0.1 Å and 14.8 ± 0.1 Å for Mg_2Ca_0Tn-C and Mg_2Ca_2Tn-C, respectively. r_{NC} was calculated to be 38.1 ± 0.5 Å and 40.5 ± 0.6 Å for Mg_2Ca_0Tn-C and Mg_2Ca_2Tn-C, respectively. The difference in physical parameters between Mg_2Ca_0Tn-C and Mg_2Ca_2Tn-C was not large but a difference does exist. In case of Mg_2Ca_2Tn-C ,however, the sample was contaminated with dimer since I(S)/C behaves like monomer-dimer equilibrium. Structural parameters are summarized in Table 4.

Table 4: Structural parameters of Tn-C in the presence of Mg^{2+}

	Ca_0Tn-C	Mg_2Ca_0Tn-C	Mg_2Ca_2Tn-C*
Rg	27.8 ± 0.3 Å	24.3 ± 0.1 Å	25.1 ± 0.1 Å
$\overline{Rg}_{N,C}$	15.4 ± 0.3 Å	15.1 ± 0.2 Å	14.8 ± 0.2 Å
r_{NC}	46.3 ± 1.0 Å	38.1 ± 0.5 Å	40.5 ± 0.6 Å
MW	22,300 ± 600	21,600 ± 500	————

* Rg and $\overline{Rg}_{N,C}$ and r_{NC} of Mg_2Ca_2Tn-C were derived from extrapolated SOXS profile. These values were not so different from the intrinsic physical parameters of Mg_2Ca_2Tn-C. Structural parameters of Ca_0Tn-C were listed again as a reference.

4. X-ray Scattering from Tryptic Fragments of Tn-C

4.a. General Features of SAXS from Tryptic Fragments of Tn-C

The scattering profiles from TR1C and TR2C are shown in Figure 19. The main difference between native Tn-C and its tryptic fragments was that SAXS profiles of tryptic fragment have no "hump" observed at 0.027 $\mathring{A}^{-1}$ in case of Tn-C. SAXS profiles of TR1C and TR2C were feature-less: they can be approximated by an exponential curve up to large scattering angle, $S \leqq 0.03\ \mathring{A}^{-1}$, irrespective of Ca^{2+}. The interference function of two domains (see APPENDIX), i.e. $\sin(2\pi r_{NC} S)/(2\pi r_{NC} S)$ was clear in SAXS profiles from native Tn-C.

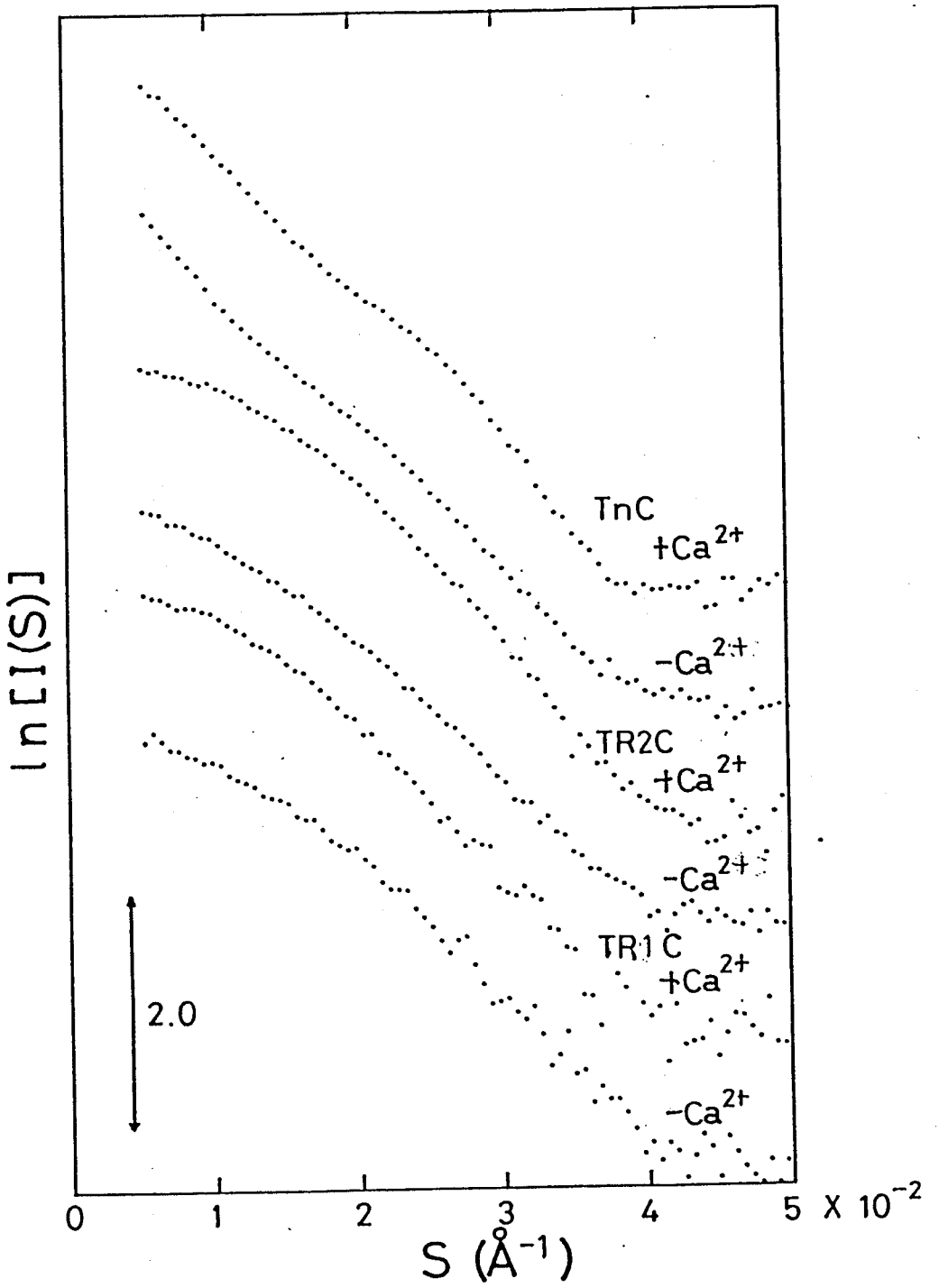

Figure 19: SAXS profiles of TR1C, TR2C and Ca_0Tn-C and Ca_4Tn-C. The interference of two domains is obvious for native troponin C molecule.

4.b. Structural Change of TR2C upon Ca^{2+} Binding

The Guinier plots of Ca^{2+}-free and Ca^{2+}-bound TR2C are shown in Figure 20. Irrespective of Ca^{2+}, the linear region (Guinier region) was very large. Interparticle interference was seen even at 12.3 mg/ml of TR2C: downward curvature in the very small angle. The Rg's obtained from the Guinier plots at different protein concentrations are plotted in Figure 21. Rg_C's (radii of gyration of TR2C) at infinitely dilute concentration was 17.0 ± 0.3 Å and 14.7 ± 0.1 Å for Ca $^{2+}$free and Ca $^{2+}$bound TR2C. Rg_C decreased greatly upon Ca^{2+}, which corresponded to the compaction of C-domain upon Ca^{2+} binding.

Forward scatterings, I(0)/C's showed a good linearity and molecular weights were estimated to be 9600 ± 900, 9000 ± 1000 for Ca^{2+}-free and Ca^{2+}-bound TR2C (in Figure 22). These values were larger by a smaller extent than 8,480 determined from amino acid sequence, which was derived from the effect of water bound to protein. The same phenomenon was seen in native Tn-C.

4.c. Structural Change of TR1C upon Ca^{2+} Binding

Guinier plots of Ca^{2+}-free and Ca^{2+}-bound TR1C are plotted in Figure 20. Characteristics of the Guinier plots were the same as those of TR2C. The dependency of Rg_N (radius of gyration of TR1C) on protein concentration was less distinctive than TR2C. Rg_N almost stays constant. Rg_N at infinite dilution was 13.9 Å ± 0.2 Å and 14.7 Å ± 0.1 Å for Ca $^{2+}$free and Ca^{2+}-bound TR1C, respectively. The Rg_N in the absence of Ca^{2+} was small, while Rg_N in the absence of Ca^{2+} had a large

value. This finding indicates that N-domain of Tn-C seems to have an ordered structure. Average radius of gyration can be calculated from these experimental values to be 15.5 Å, which is in accordance with the $\overline{Rg}_{N,C}$ obtained from S^2-ln{I(S)} plot. Binding of Ca^{2+} increased Rg_C. Molecular weights of TR1C were determined to be 8000 ± 200 and 10600 ± 300 for Ca^{2+}-free and Ca^{2+}-bound TR1C, respectively. The molecular weight of Ca^{2+}-bound TR1C was a little larger than Ca^{2+}-free TR1C. Since both I(0)/C and Rg_C increased upon Ca^{2+} binding, binding of Ca^{2+} may cause an aggregation of TR1C. The topic will be discussed further later.

Table 5: Structural parameters of tryptic fragments of Tn-C in different states

		Rg_N and Rg_C (Å)	molecular weight
TR1C	$-Ca^{2+}$	13.9 (0.2)	8,100 (300)
	$+Ca^{2+}$	15.0 (0.1)	10,600 (100)
TR2C	$-Ca^{2+}$	17.0 (0.3)	9,600 (900)
	$+Ca^{2+}$	14.7 (0.1)	9,000 (1,000)

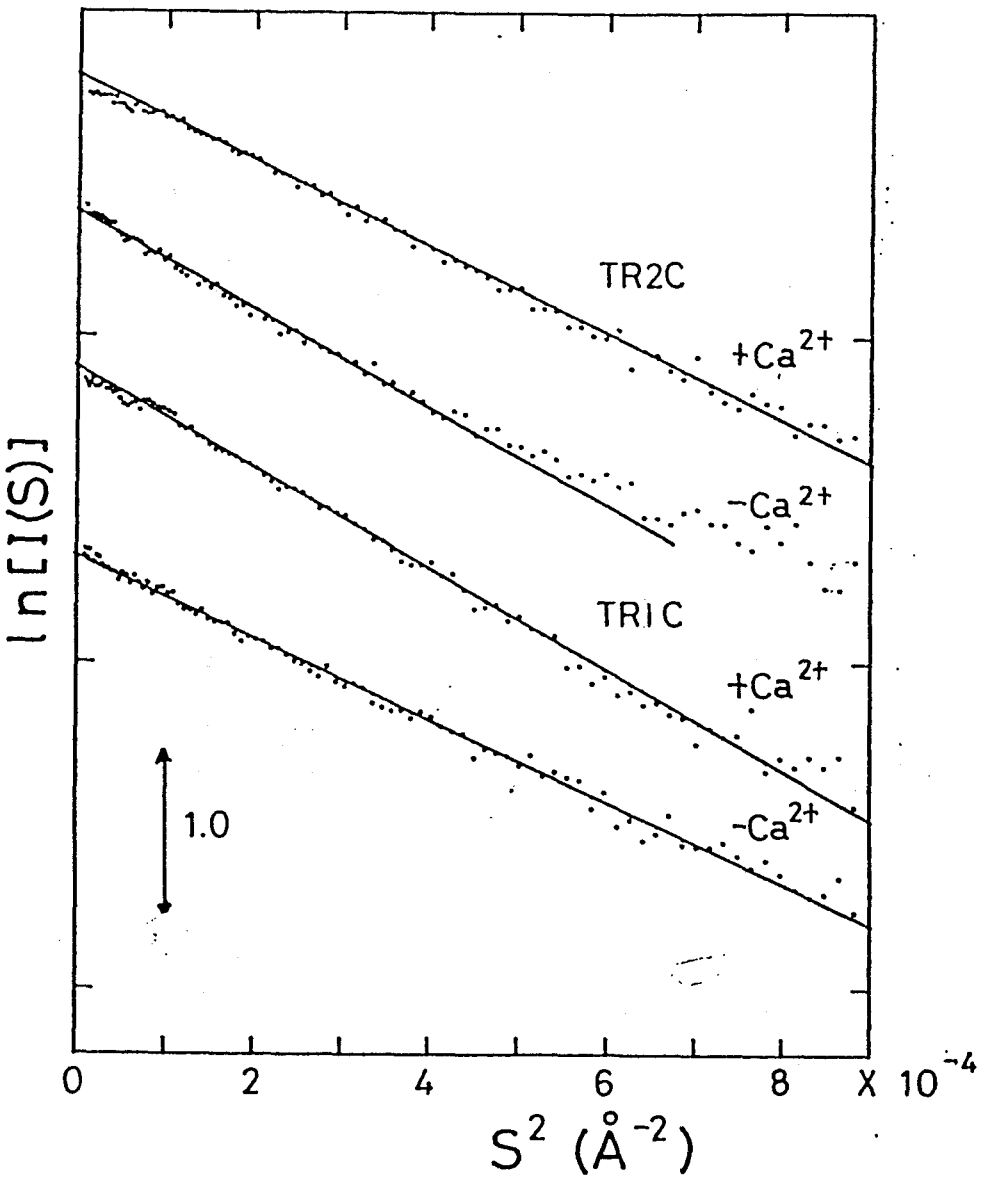

Figure 20: Guinier plots of tryptic fragments of Tn-C, TR1C and TR2C. Except for a small deviation for Ca^{2+}-free TR2C, tryptic fragments of Tn-C is well approximated by Gaussian function.

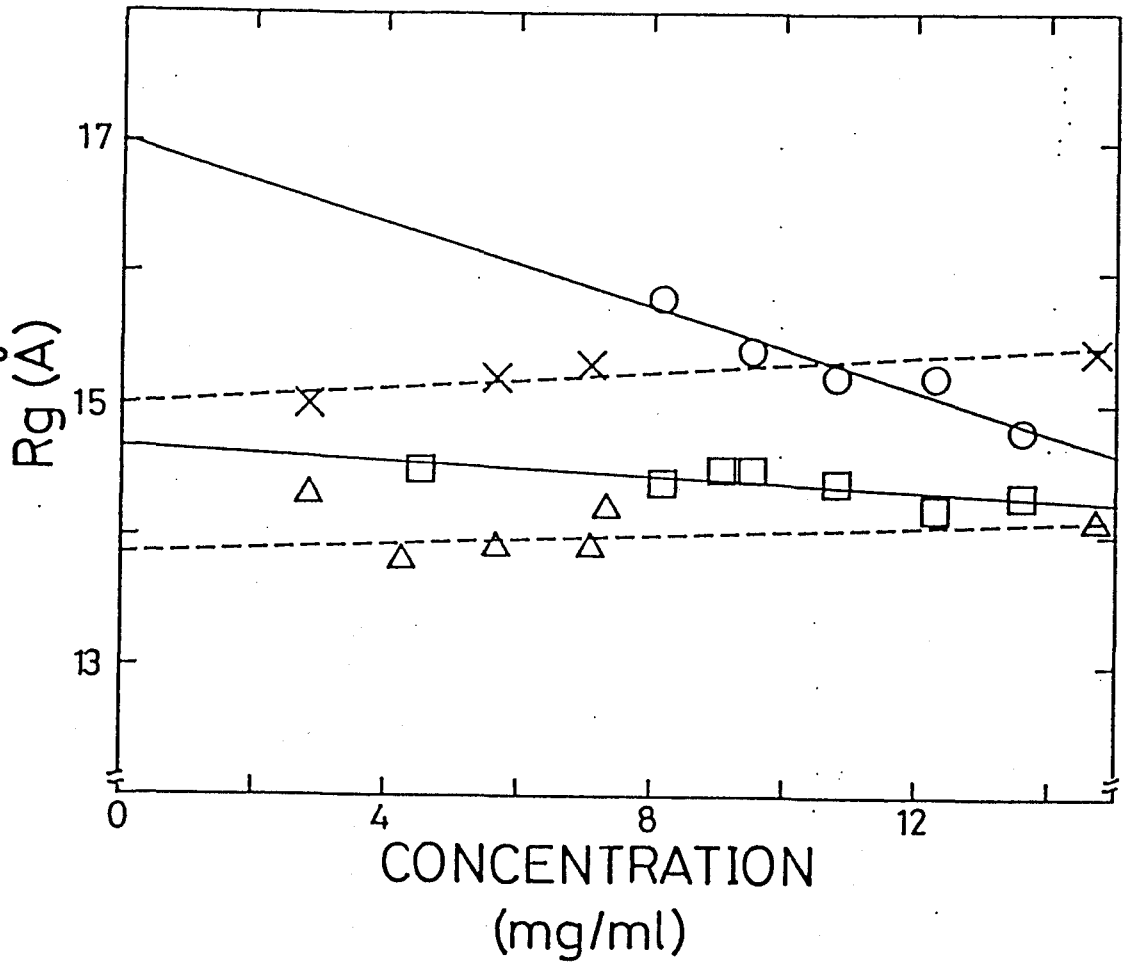

Figure 21: Protein concentration dependence of Rg_C's and Rg_N's for Ca^{2+}-free TR2C (○), Ca^{2+}-bound TR2C (□), Ca^{2+}-free TR1C (△) and Ca^{2+}-bound TR1C (×).

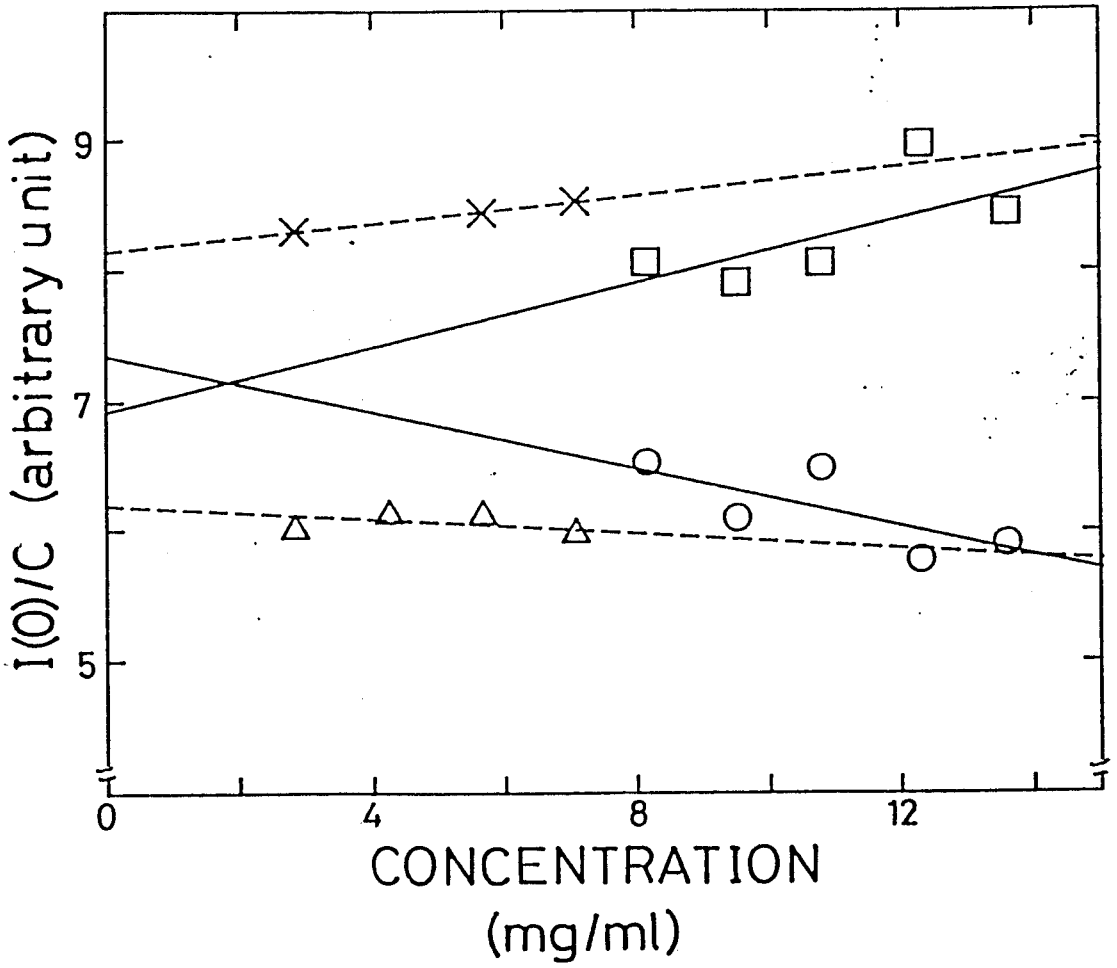

Figure 22: Protein concentration dependence of forward scattering, I(0)/C, obtained from the Guinier plot approximation for Ca^{2+}-free TR2C (○), Ca^{2+}-bound TR2C (□), Ca^{2+}-free TR1C (△) and Ca^{2+}-bound TR1C (×).

5. SOXS Profile Based on the Molecular Structure of Tn-C in the Crystalline State

A SOXS profile of the Tn-C molecule, calculated from the atomic coordinates in the crystalline state, is shown in Figure 23. The atomic scattering factor used was corrected for solvent inaccessible volume. The contrast of the particle was determined fitting with an experimental curve.

A characteristic of the calculated SAXS profile of Tn-C was that a "hump" existed at $S = 0.027\ \mathring{A}^{-1}$. This was always seen irrespective of the contrast, although the position of the hump changed with the contrast. This characteristic is consistent with experimental profiles (Figures 7 (a), (b)). Nevertheless the discrepancy between calculated intensity and experimental profiles was evident: the experimental profiles shifted to smaller scattering angles than the calculated one. These results indicate the homology of the structure in solution to that in crystal, but there is the difference in size between two states.

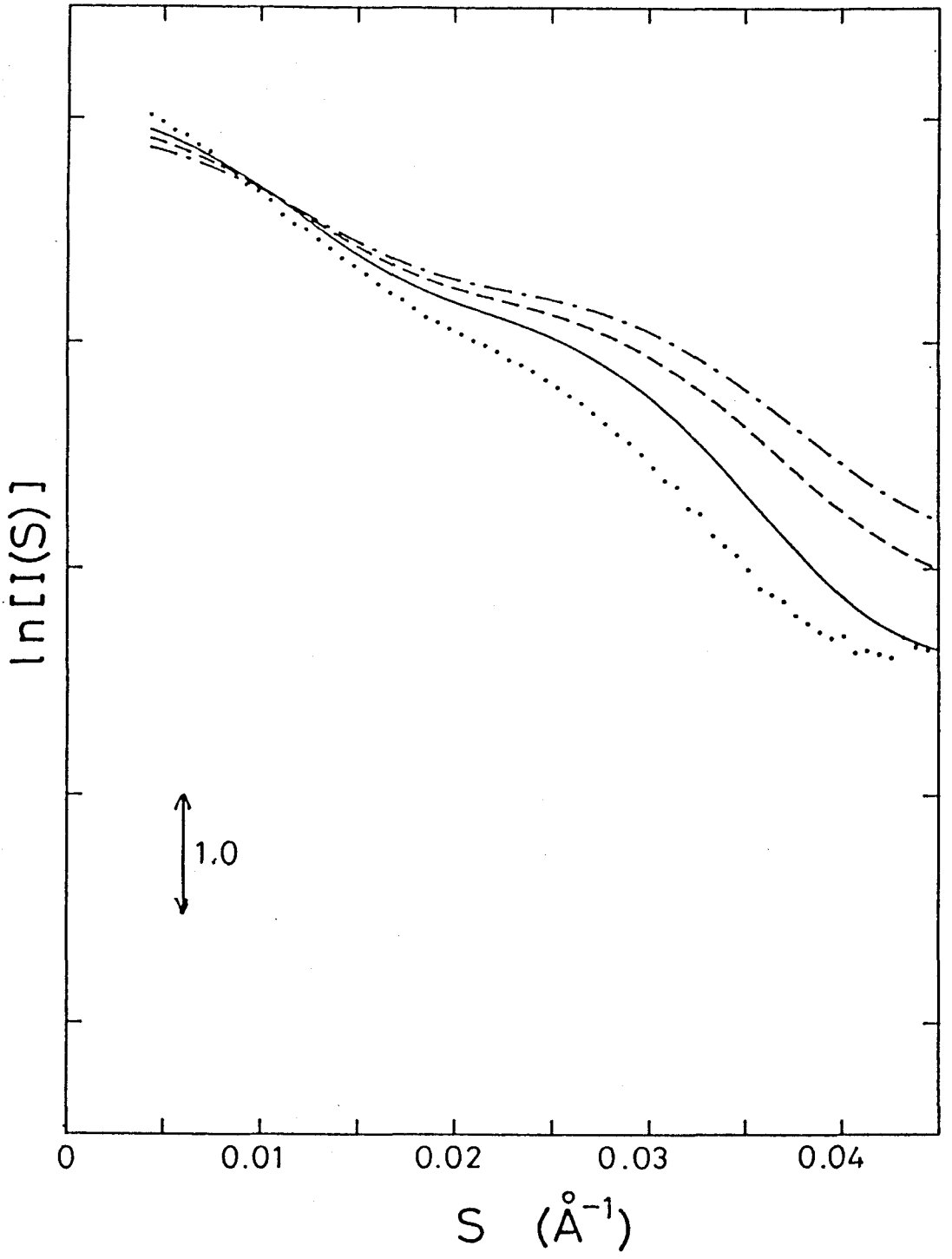

Figure 23: The dotted line represents the experimental SOXS profile of Ca_2Tn-C in solution. The other lines are SOXS profile calculated from amino acid coordinates in crystalline state with various solvent densities; zero (solid line), 2 (broken line) and 3 (chain-dotted line). The calculated intensity cannot be fitted to the experimental curve.

The difference is much more clear in tryptic fragments of Tn-C. SAXS profiles of the tryptic fragments also showed the shift of SAXS profile to smaller angles (Figure 24). P(r) obtained from amino acid coordinates indicated that the size of each domain was apparently more expanded than the crystal structure (Figure 25).

Physical parameters also supported the above hypothesis. Rg's from direct calculation from the coordinates in crystalline state was 22.9 Å, 12.4 Å and 12.5 Å for Rg and Rg_C and Rg_N, respectively. These values were smaller than experimental values. The distance between two domains of the crystalline structure was similar but the size of each domain was smaller than the structure in solution.

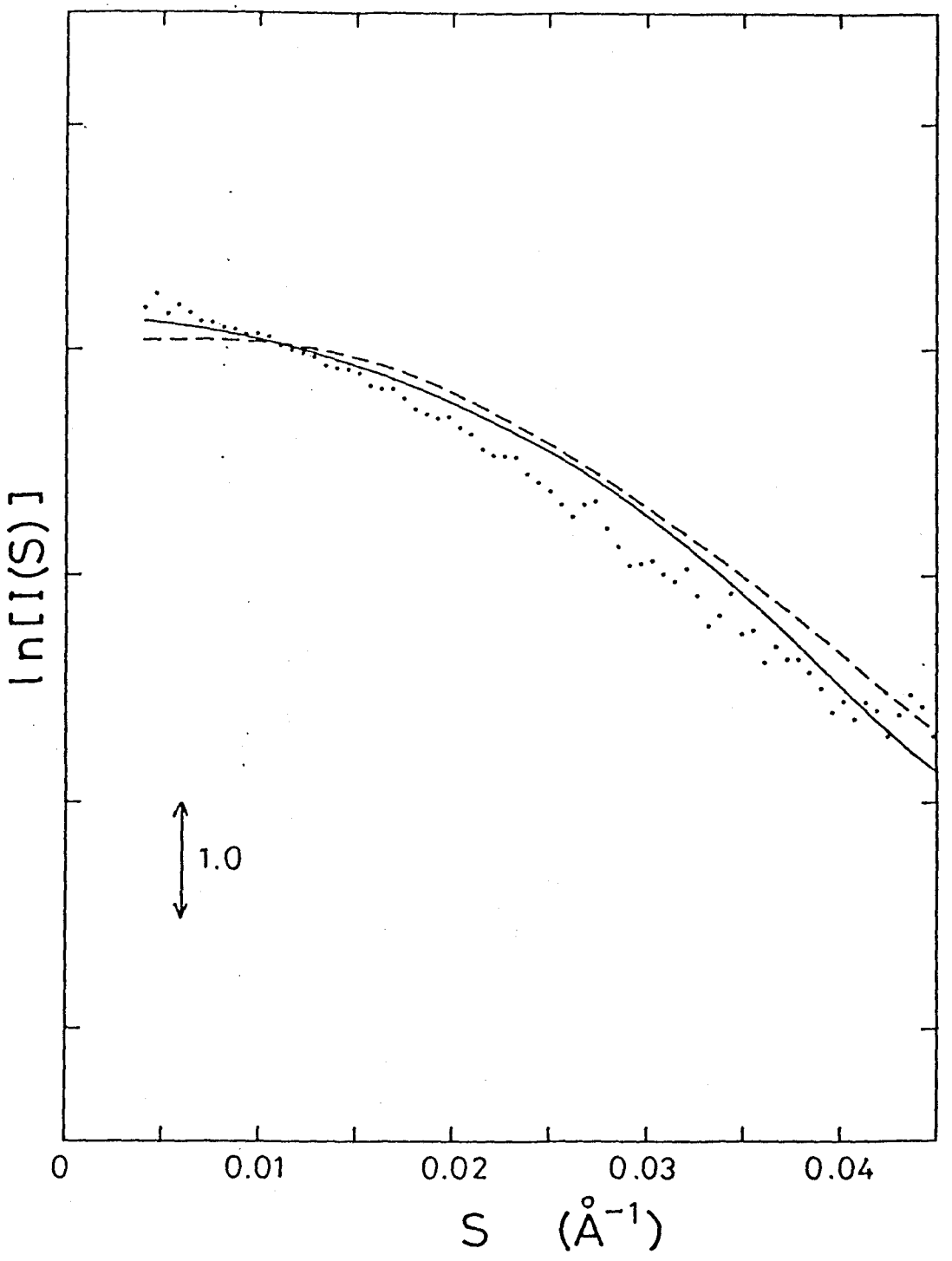

Figure 24 (a): SAXS profile calculated from the structure of TR1C in crystalline state. The dotted line represents Ca^{2+}-free TR1C. Symbols are the same as in Figure 23.

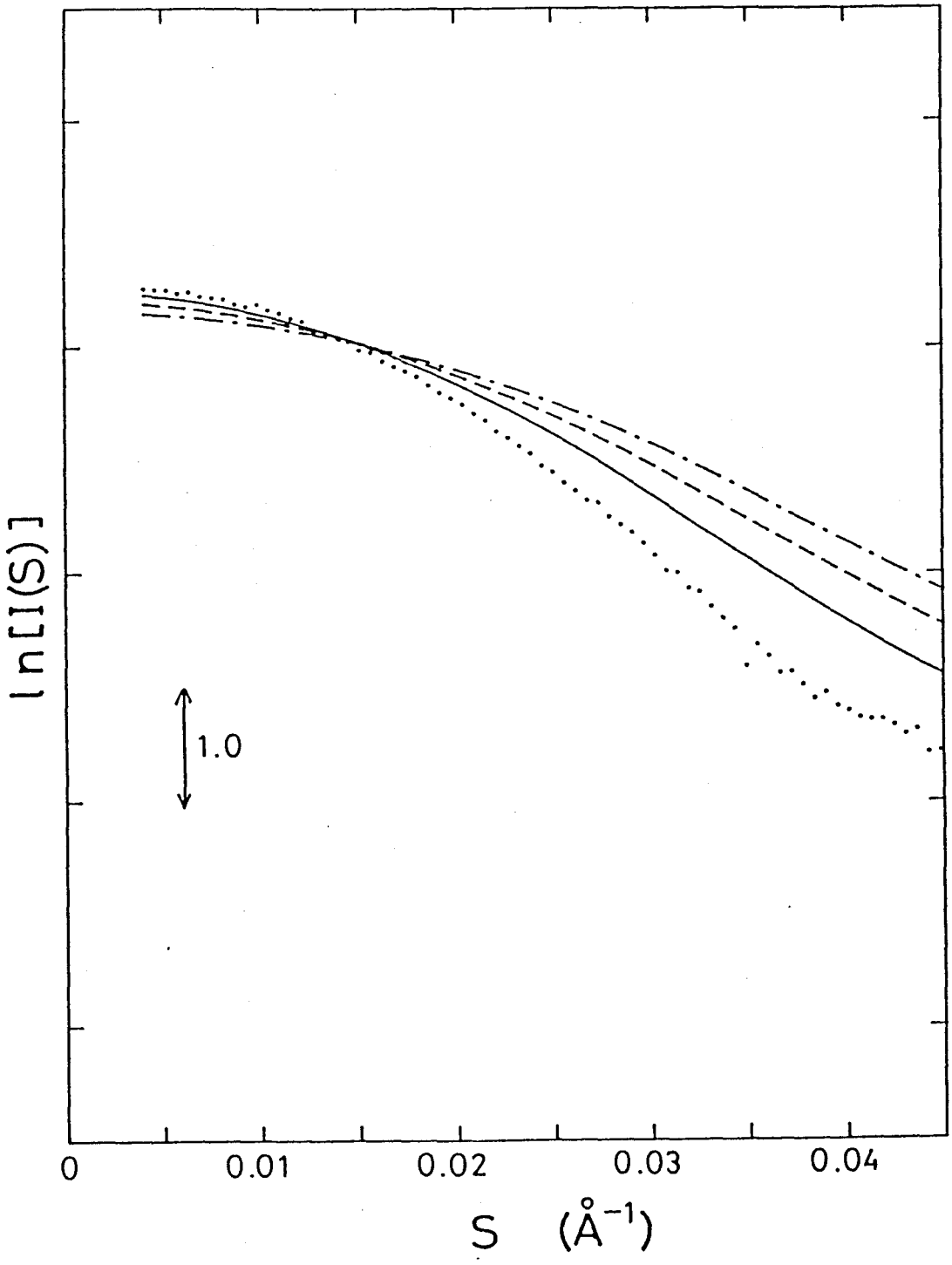

Figure 24 (b): SAXS profile calculated from the structure of TR2C in the crystalline state. The dotted line represents Ca^{2+}-bound TR2C. Symbols are the same as Figure 23.

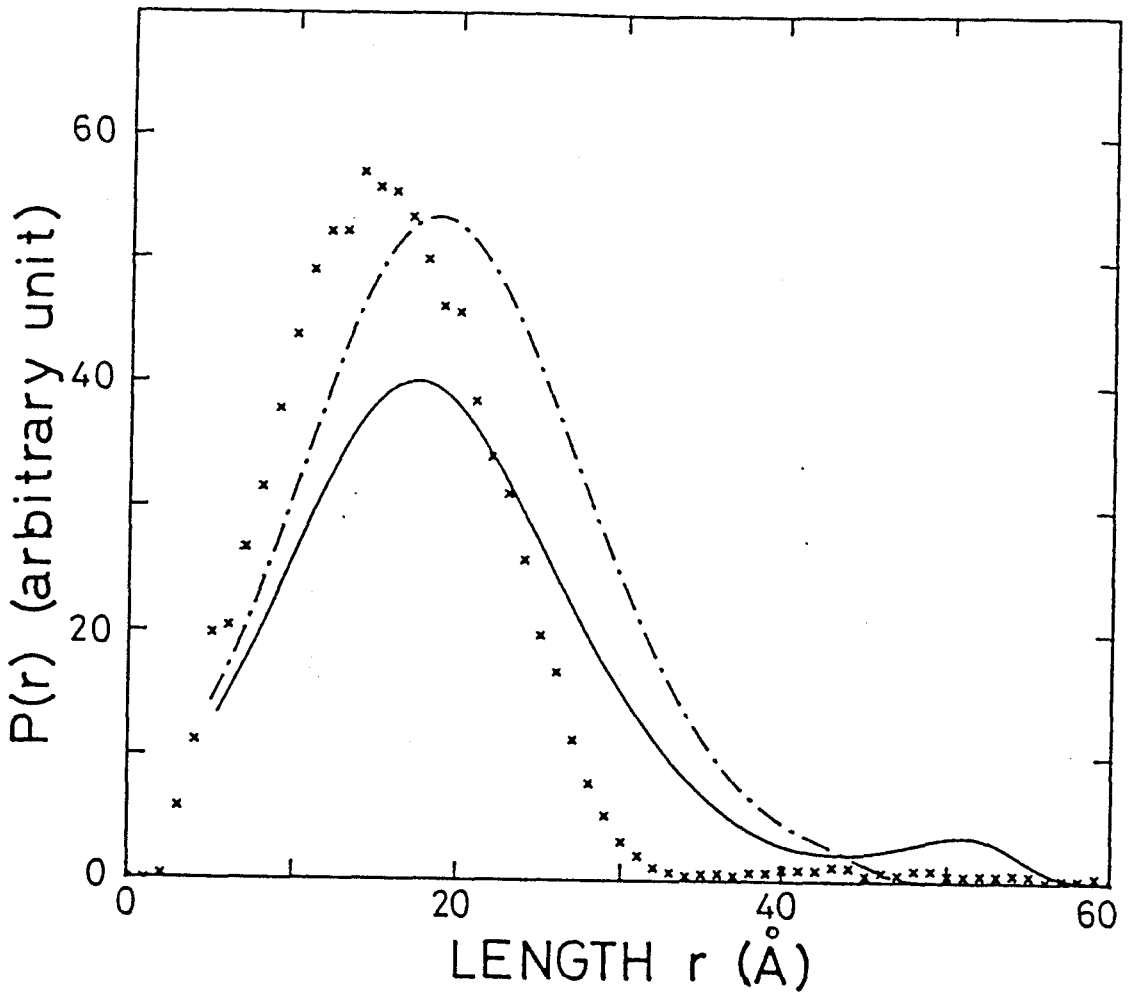

Figure 25 (a): Distance distribution function of TR1C: Ca^{2+}-free TR1C (solid line), Ca^{2+}-bound TR1C (chain-dotted line) and crystal structure calculated by amino acids coordinates (x).

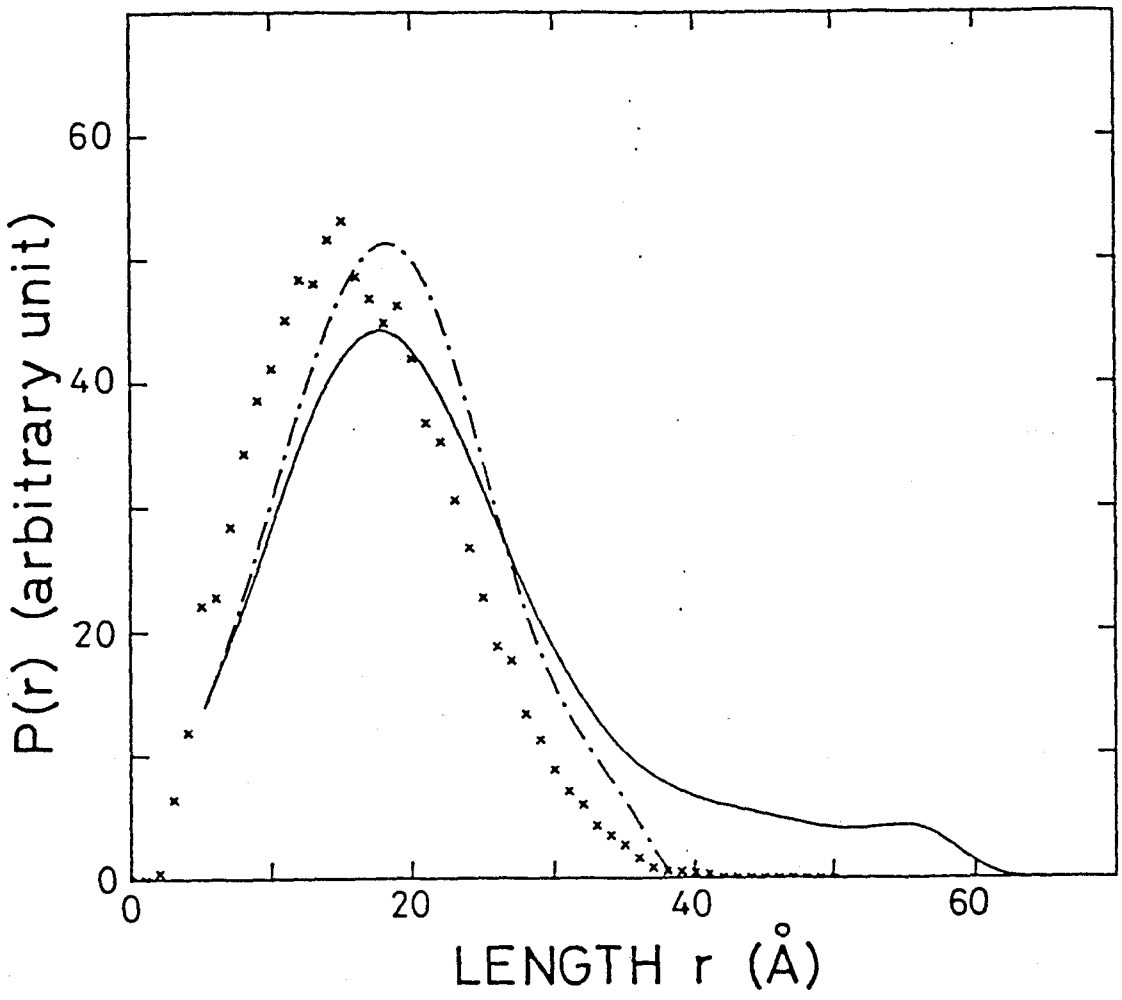

Figure 25 (b): Distance distribution function of TR2C: Ca^{2+}-free TR2C (solid line), Ca^{2+}-bound TR2C (chain-dotted line) and crystal structure (x).

DISCUSSIONS

1. Aggregation State of Tn-C

1.a. Interparticle Interference

In the present study, the author is mainly concerned with the structural change of Tn-C upon Ca^{2+} binding. For this purpose, SAXS profiles of Tn-C have to be from monodisperse Tn-C and the interparticle interference effect must be extracted to obtain the intrinsic scattering profile.

The preliminary SAXS experiment on Tn-C implied serious interparticle interference, a downward curvature of the SAXS profile in the inner region of scattering even at a concentration of 20 mg/ml (36). SAXS experience therefore had to be performed on dilute solutions down to 2 mg/ml, and from these profiles It was possible to obtain the intrinsic scattering profiles of the Tn-C in various states extrapolating to infinitely diluted solutions, as described in RESULTS.(Figures 9 and 15)

1.b. Aggregation State of Tn-C

As to the aggregation of the Tn-C molecule, there have been several reports and they can be classified into two contradictory reports. The first represented by Marggossian and Stanford (34) reported that extensive dimerization occurred even in the presence of EGTA and this effect was enhanced on binding of Ca^{2+} to Tn-C. On the other hand, Murray and Kay (16) found very little aggregation effect below pCa 4.0 and apparent dimerization in the presence of millimolar Ca^{2+}. In view of the SAXS

experiment, serious aggregation of molecules in solution would result in upward curvature of the SAXS profile in the inner part of scattering on Guinier plot. This is not true in the present case, as is evident in Figures 8 and 14.

The fraction of the dimer in the solution also depends on the concentration of protein since it is determined from the equilibrium between monomer and dimer. Firstly, since the contamination changes the forward scattering intensity, I(0)/C should increase as the Ca^{2+} concentration increases. Secondly, the plots of I(0)/C or Rg *vs.* concentration of Tn-C deviate from a straight line if the fraction of the dimer increases with the concentration of Tn-C. The present SAXS experiment indicates that the I(0)/C's do not change for all states of Tn-C except Mg_2Ca_2Tn-C, and the I(0)/C and Rg dependences on the concentration also are not in favor of contamination with dimer. The P(r) function also provides information about the small amount of aggregation effect on SAXS *via* indirect transformation methods (56). Such information comes from a series of calculations of Rg values as a function of the maximum length, D_{max}, at minimum reciprocal fitting parameters S_{min}. If the Rg value at small S_{min} values increases monotonously with an increase in D_{max} and reaches a plateau at some S_{min} value, aggregation of the molecule is expected in the sample solution. This method also indicated that there is no dimer contamination except Mg_2Ca_2Tn-C.

In case of Mg_2Ca_2Tn-C however I(0)/C increases over the range of 2-6 mg/ml, which suggests contamination with dimer.

The author tried to explain this by a dimer-monomer model in which a linear concentration dependency of apparent I(0)/C is assumed. Best fit parameters by least-squares method are 511 M^{-1} of apparent dimerization constant. The estimated values of I(0)/C were plotted in Figure 17. The expected fraction of dimer at experimental concentrations are shown in the table below.

Table 6: Expected fraction of Mg_2Ca_0Tn-C dimer at experimental protein concentrations

protein concentration (mg/ml)	monomer (%)	dimer (%)
2	97.4	2.6
3	93.1	6.9
4	91.3	8.7
6	88.2	11.8
8	85.5	14.5
10	83.2	16.8

At first glance this finding is incompatible with the good linearity of scattering profile in Guinier plot and Rg dependence on protein concentration. This contradiction is due to the difference between Eq (12) and Eq (13): Normally, Rg of a dimer is much larger than that of a monomer so that contamination with dimer becomes conspicuous both in the Guinier plot and in I(0)/C. If the Rg of a dimer is not so different from that of a monomer, the all the results can be explained Tn-C has an elongated structure or dumbbell structure; it is possible to think a plausible configuration without changing the structure of each

domain. When two Tn-C are deposited in line, for example, Rg of the Tn-C is larger than that of the monomer by 60 %. However, when the four domains are placed in a tetrahedral arrangement, which gives the smallest value of Rg, Rg of the dimer is larger than that of the monomer by only 24 %. In this case the good linearity of Guinier plots and the dependency of Rg on protein concentration can be well explained, since the ratio of dimer content is probably up to 20 % of the total Tn-C at 10 mg/ml. From the restriction of the good linearity on Guinier plots, Mg_2Ca_2Tn-C dimer exists as a compact configuration, such as a tetrahedral arrangement.

Thus, the SAXS profiles in the present study are taken as of a monomer solution of Tn-C except Mg_2Ca_2Tn-C. These conclusions allowed us to analyze the SAXS profiles to detect the structural change of Tn-C upon binding of Ca^{2+} and Mg^{2+} to high affinity sites.

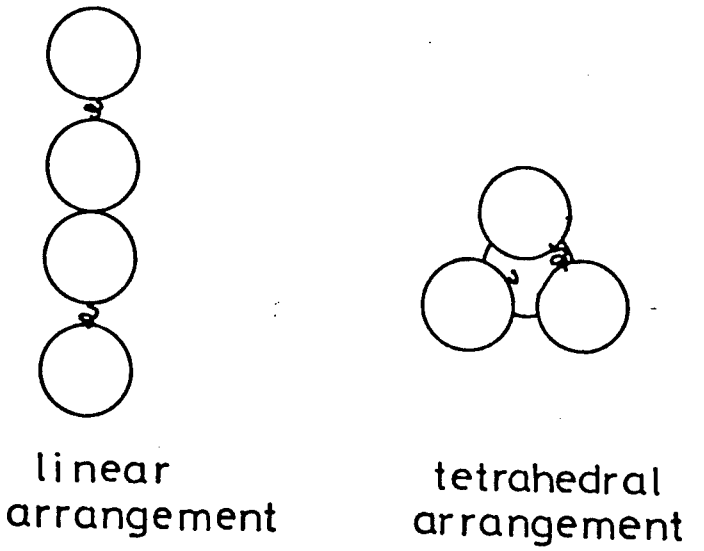

Figure 26: Schematic picture for two types of arrangements of the dimer. Each circle represents the domain of Tn-C.

1.c. Molecular Weight of Tn-C

I have to add a remark on the molecular weights of Tn-C that are presented in RESULTS. Instead of performing an absolute measurement of scattering intensity, I carried out a relative method to estimate the molecular weight using lysozyme as a reference. This method is accurate if several conditions are met: the two proteins must have similar shape, the same surface properties with regard to hydration and the same partial specific volume (i.e., the same Δz [electron density difference]). The present value, ~22.000 irrespective of Ca^{2+} concentration except Mg_2Ca_2Tn-C, is higher than the value calculated from the amino acid sequence. A simple-minded interpretation might erroneously lead to a calculation of the amount of dimer in solution, i.e., about 20 %. However, it is hardly understandable that the degree of contamination stays at a certain level, independent of the Ca^{2+} concentration. This discrepancy can be rationalized in two respects (see Eq.[11]). One of the differences is in the excess electron density of molecules, Δz. Only one percent difference in density, which seems very probable, causes a difference in I(0)/C of as much as about ten percent. Hence this may be the major factor. The other factor is the number of water molecules bound to the protein. If the shape and properties of the surface are not different from each other, the degree of hydration is the same for these molecules. However, the Tn-C molecule being dumbbell-shaped, it has a larger surface area per unit volume than lysozyme. Besides, the Tn-C molecule carries more charged groups than lysozyme under the experimental

conditions, as judged from the amino acid sequence: at pH~7, there are 21 negative and 8 positive charges in the N-domain and 20 negative and 7 positive side chains in the C-domain. The lysozyme molecule has only 18 positive side chains and no negative side chains at pH 3.8 (Fujisawa, T. & Ueki, T., unpublished calculation). The Tn-C molecule, therefore, is expected to be more hydrated than the lysozyme molecule, and the estimated molecular weight therefore tends to be larger than the value calculated from the amino acid sequence. The same conclusion was employed by Murray and Kay. Molecular weights of tryptic fragments (~9500 is larger than 8500 from amino acid sequence) is also in accordance with the above speculations.

2. SOXS from Tn-C

As described in RESULTS, scattering from Tn-C has a hump at 0.027 $\mathring{A}^{-1}$, while tryptic fragments do not have this feature (Figure 19). It is evident that this characteristic derives from interference of two domains rather than the internal structure of each domain. The pair distribution function indicates the two-domain structure more clearly. It resembles the pair distribution of two ellipsoids demonstrated by Glatter et al. (51). It is natural that at low resolution a dumbbell structure can be represented by two domains.

The characteristics of P(r) function are the same for all states of Tn-C so that this dumbbell structure remains even for Mg_0Ca_0Tn-C, although the extended structure is supposed from the maximum dimension of P(r) function. So the analysis based on the dumbbell structure described in APPENDIX is valid for all

states of Tn-C.

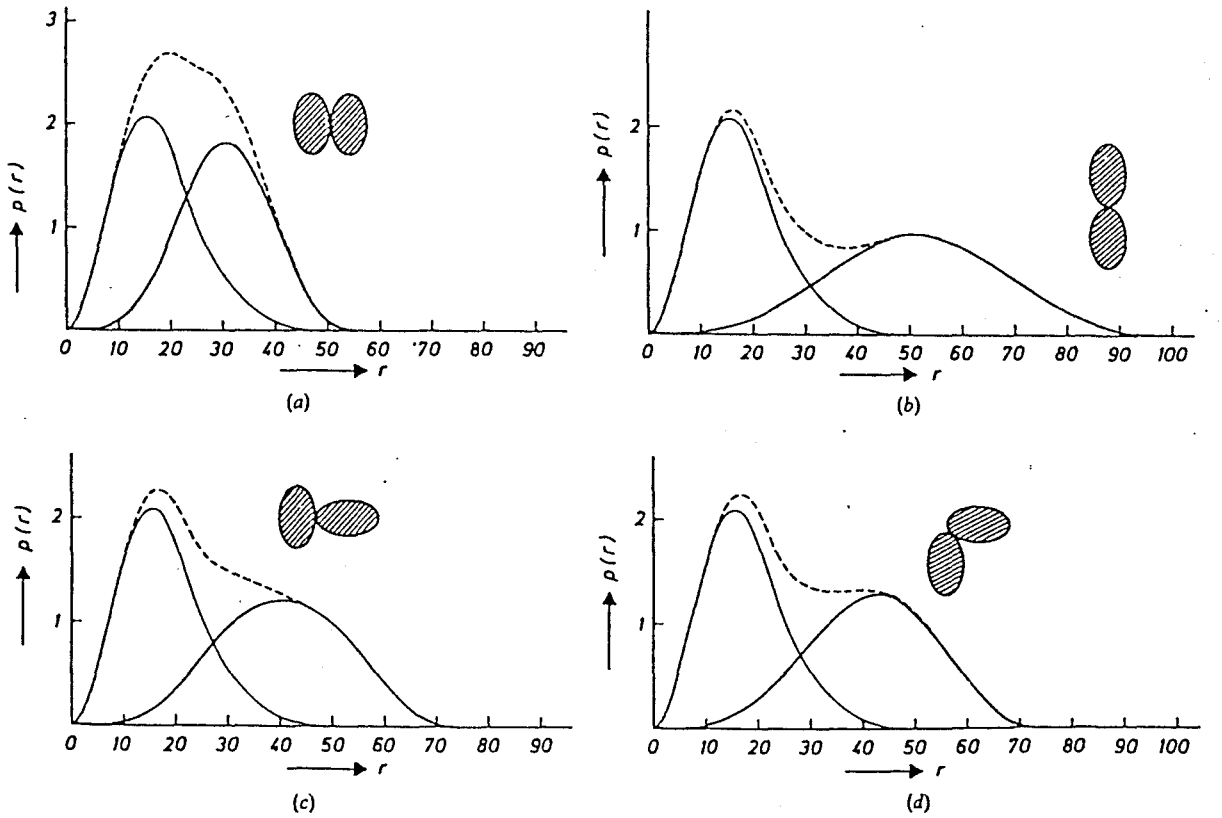

Figure 27: Distance distribution function, P(r), from two domain model built from prolate ellipsoids: solid line; one domain, broken line; two domain, bold line; difference between two functions. (a) parallel formation, (b) linear formation, (c) T-type, (d) L-type calculated by Glatter, O. (51).

3. Structural Change upon Ca^{2+} or Mg^{2+} Binding

3.a. Structural Change upon Ca^{2+} Binding in the Absence of Mg^{2+}

In this section the author will describe the structure of Ca_0Tn-C, Ca_2Tn-C and Ca_4Tn-C. In the absence of Ca^{2+} and Mg^{2+}, Tn-C molecule has a large asymmetry, i.e., an elongate structure, which was reflected by a large value of Rg and D_{max} of Tn-C. Rg of other spherical protein such as α-chymotrypsin (molecular weight is 24,500) is 18.0 Å (57), while that of Ca_0Tn-C was 27.8 Å. Large D_{max} of Tn-C is also in accordance with this results. The structure of Tn-C in solution , though is supposed to keep dumbbell structure. The domain of Ca^{2+}- and Mg^{2+}-free Tn-C is rather expanded from the maximum length, D_{max} of the fragments and $\overline{Rg}_{N,C}$. Especially in the absence of Ca^{2+}, C-domain is considerably unfolded since both the D_{max} of TR2C and Rg_C is large, while N-domain already has an ordered structure which is expected from $\overline{Rg}_{N,C}$ and P(r).

Binding of Ca^{2+} to high affinity sites brings about the compaction of C-domain, Rg_C decreases by 2.3 Å so that the decrease of $\overline{Rg}_{N,C}$ is mainly attributable to C-domain. The length in r = 40-60 Å of P(r) function of TR2C decreased considerably upon Ca^{2+} binding. This compaction of domain is parallel to the decrease in r_{NC}, which was indicated by decreases in Rg, $\overline{Rg}_{N,C}$, and r_{NC}. A decrease in the dependency on protein concentration of physical parameters corresponds the decrease in the exclusion volume of Tn-C, i.e., asymmetry of Tn-C decreased. The results indicate that Tn-C molecule contracts along its long

axis.

With further binding of Ca^{2+} to low affinity sites, the Tn-C the contraction continues but not to as greater as binding of Ca^{2+} to high affinity sites. $\overline{Rg}_{N,C}$ does not decrease very much but shortening of r_{NC} by a few angstroms was observed. Rg_N increased whereas it is supposed to decrease. It is quite doubtful whether the increase has a physiological meaning. This contradiction comes from the deficiency of first ten amino acids which was reported to play an important role in domain interaction suggested by NMR resonances (29).

3.b. Structural Change of Tn-C upon Ca^{2+} Binding in the Presence of Mg^{2+}

In high affinity sites (C-domain), binding affinity of Mg^{2+} is higher than Ca^{2+} (table 1) consequently in the presence of few millimolars of Mg^{2+} (physiological condition) Tn-C carries two Mg^{2+} in C-domain. Binding of Ca^{2+} to Tn-C occurs mainly at Ca^{2+} specific sites (N-domain).

Firstly, the binding of Mg^{2+} to high affinity sites will be discussed. All SAXS parameters of Mg_2Ca_2Tn-C were smaller than the Ca^{2+} and Mg^{2+}-free Tn-C (Ca_0Tn-C) just like in the case of Ca_2Tn-C. The $\overline{Rg}_{N,C}$ and r_{NC} decreases, which shows the domain become compact with the shortening of the domain distance. Structural parameters of Mg_2Ca_0Tn-C are similar but not identical to Ca_2Tn-C , i.e., all parameters are larger by 2 %. This result could be a reflection of a small difference between the two structures, Mg_2Ca_0Tn-C and Ca_2Tn-C: each domain, probably C-

domain and the r_{NC} of Mg_2Ca_0Tn-C is larger than Ca_2Tn-C. In spite of these small differences, the overall structure of Mg_2Ca_0Tn-C undoubtedly resembles to that of Ca_2Tn-C. The Rg and I(0)/C dependence on protein concentrations, which is related to surface property and whole structure, is not so different. As described in INTRODUCTION this is in good accordance with the other results reported by spectroscopical methods and thermostability.

Analysis of the SAXS profile from Mg_2Ca_2Tn-C is very difficult since forward scattering, I(0)/C increased with increasing protein concentration in 2-6 mg/ml. As described previously Mg_2Ca_0Tn-C is supposed to dimerize with apparent dimerization constant 511 M^{-1}. Even if the dimerization occurs, the fraction of dimer is effectively low at 3 mg/ml (less than 3 %) so that the extrapolation of the apparent SAXS profiles in 3-6 mg/ml to infinite dilution does not lead to a serious deviation from the intrinsic SAXS profiles. Structural parameters of Mg_2Ca_0Tn-C from extrapolated SAXS profiles could adequately reflect the intrinsic structure.

Ca^{2+} binding to low affinity sites cause an increase in Rg in the presence of Mg^{2+} and a decrease in Rg in the absence of Mg^{2+}, respectively. This is the reverse direction of structural change, which indicates that structure of the Tn-C molecule varies with Ca^{2+} differently in the presence of Mg^{2+}. This difference is mainly attributable to a 2-Å increase in r_{NC}, since $\overline{Rg}_{N,C}$ remains constant irrespective of Mg^{2+}.

As a summary of this section, schematic pictures of structural changes of Tn-C upon Ca^{2+} or Mg^{2+} binding was

conceptualized in next page. This picture is taken account of the present results as well as the other results obtained by other techniques.

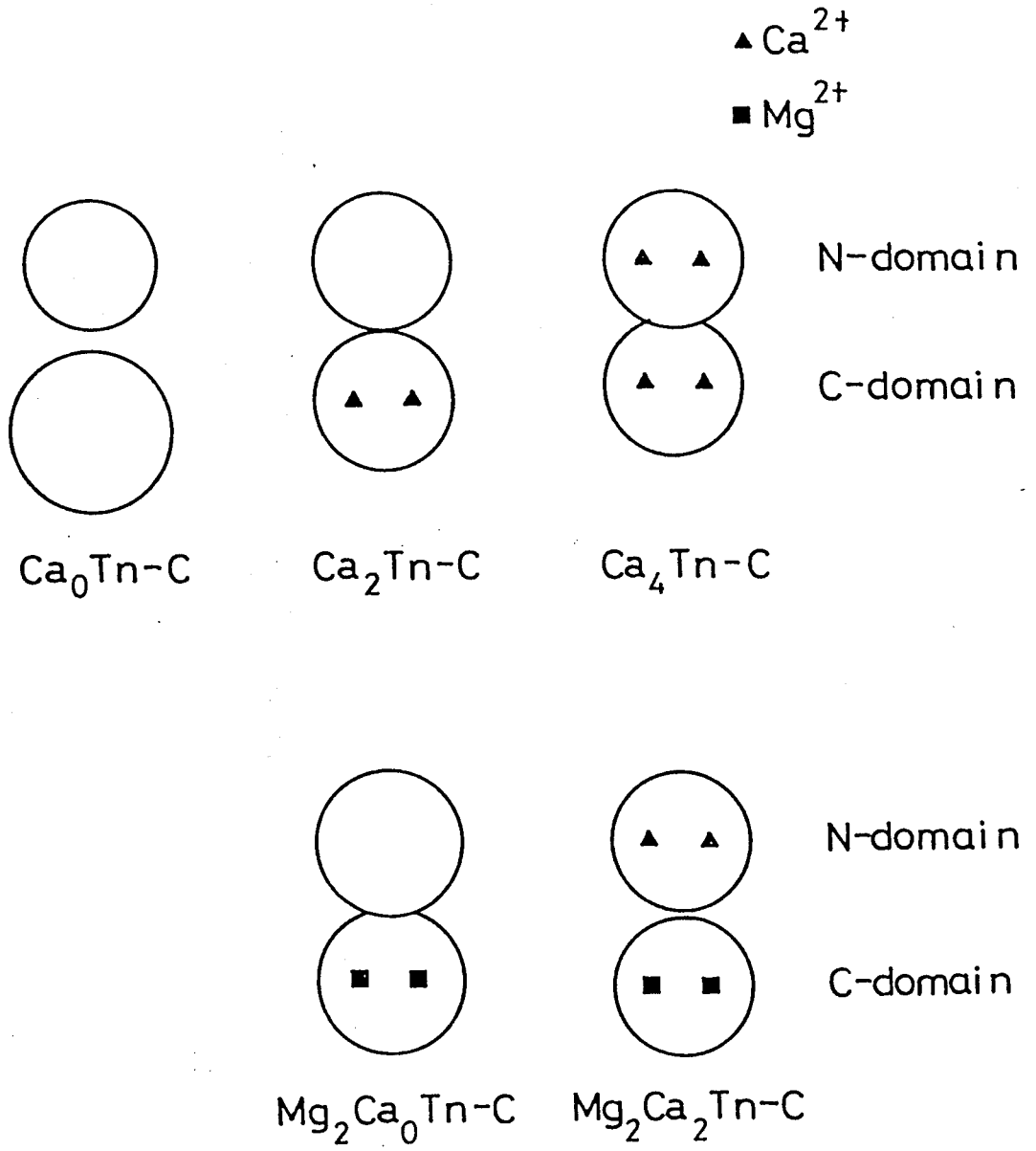

Figure 28: Schematic picture for structural change of Tn-C upon Ca^{2+} or Mg^{2+} binding. The structural change of Tn-C was conceptualized on the basis of the present results.

4. Comparison of the Results with Those Obtained by Other Techniques

In this section we compare our SAXS results with those obtained from other techniques.

The Ca^{2+}-induced change in Rg and $\overline{Rg}_{N,C}$ is quite comparable with the results of CD measurement and proton NMR studies (1,2), as described in INTRODUCTION. The Stokes radius of Tn-C decreases from 26.3 Å to 24.3 Å upon Ca^{2+} binding (17), comparable to the decrease of Rg of the molecule (see Table I). The decrease in $\overline{Rg}_{N,C}$ upon Ca^{2+} binding to the high affinity sites is also consistent with the increase in α-helix content, i.e., the domain becomes more compact. The Tn-C molecule becomes more stable against temperature upon Ca^{2+}, which also corresponds with the present results. The decrease of the interdomain distance, the Ca^{2+}-induced contraction of Tn-C, is comparable with the decrease in viscosity. Nevertheless, there also exist contradictory experimental data by the fluorescence energy transfer method to the effect that the distance between Met-25 and Cys-96 is insensitive to binding of Ca^{2+} or Mg^{2+} ions (32,33). The uncertainty of the position of the probes could lead to this discrepancy.

There are also several lines of study on structural change of Tn-C upon Ca^{2+} binding to Tn-C in the presence of Tn-C. α-helical contents measured by CD of Mg_2Ca_0Tn-C is identical with Ca_2Tn-C. PMR resonances suggests Mg_2Ca_0Tn-C is more unfolded than Ca_2Tn-C. The fluorescence of the probe attached to Cys-98 in C-domain is completely different between Mg_2Ca_0Tn-C and Ca_2Tn-

C. Thermostability of Mg_2Ca_0Tn-C is slightly lower than Ca_2Tn-C. These facts is identical with the present results. The most interesting finding of the present results is that the structural change upon Ca^{2+} binding to N-domain is completely different between in the presence and absence of Mg^{2+}; in the presence of Mg^{2+} the domain becomes compact in parallel to the increase of the distance between two domains. The results reported by other methods such as CD, NMR and PMR spectra also observed the tightening of Tn-C so that they concluded the identical structure between Ca_4Tn-C and Mg_2Ca_2Tn-C. These measurements are affected by local conformation of Tn-C rather than by overall structure. The present results could be compatible with them.

5. Comparison of the Present Results with Those of the Other SAXS Experiments

Since our first article concerning SAXS from Tn-C was published in 1987, two articles were published by Heidorn and Trewhella and Hubbard et al. (30,31). They also observed characteristics of I(S) and P(r) from a dumbbell structure, though there are many discrepancies. The main difference lies in the structure and structural change upon Ca^{2+} or Mg^{2+} binding.

Hubbard et al. reported that Rg was 23.2 Å, 22.8 Å, and 23.0 Å for Ca_0Tn-C, Ca_2Tn-C and Ca_4Tn-C, respectively (30). The dependences of the Rg's and forward scatterings on protein concentration were smaller than ours. They once observed the slight upward curvature in Guinier plot, which has never been observed in our experiments.

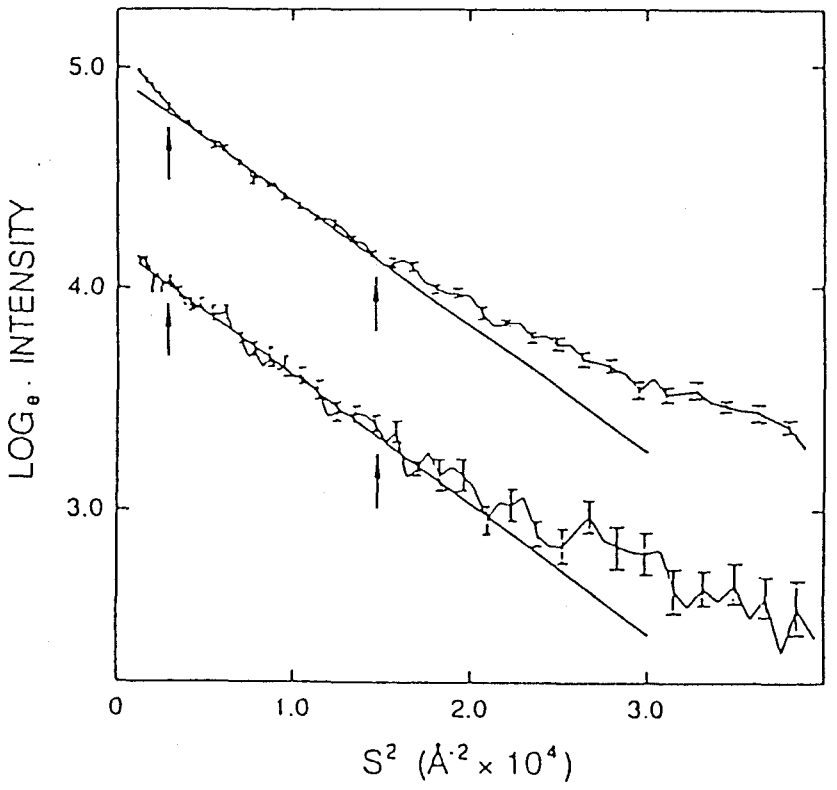

Figure 29: Guinier plots and fits for Ca_4Tn-C presented by Hubbard et al. (30). The two plots are taken from different experiments. The upward curvature is clear at top. The fitting ranges are indicated by the arrows.

Both forward scattering, apparent I(0) and Rg of Tn-C at 26.4 mg/ml increased with increasing Ca^{2+} and they concluded the apparent aggregation caused by Ca^{2+} binding. Their values of Rg's are cited in next page.

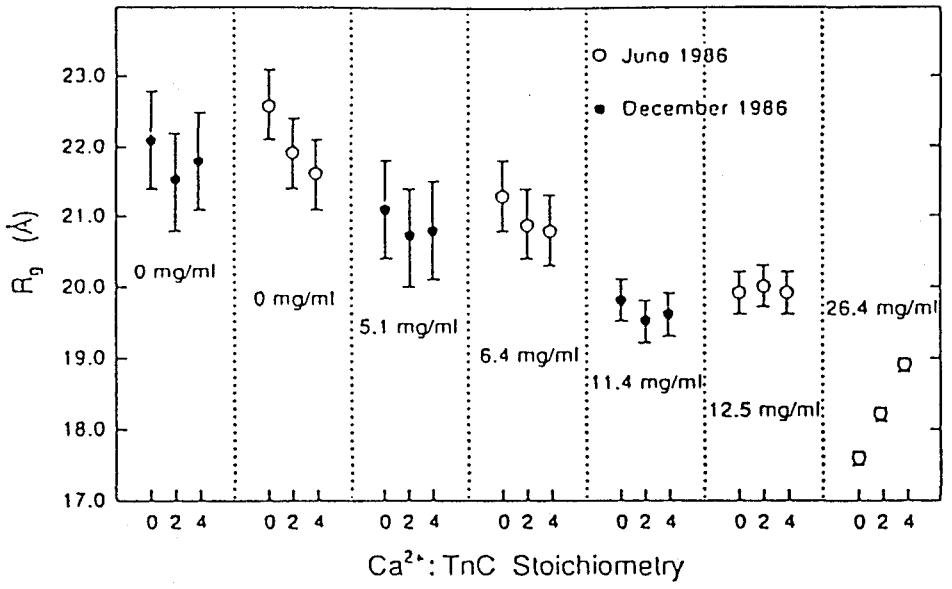

Figure 30: Rg as a function of Ca^{2+} and protein concentration by Hubbard et al. (30)

The principal reason of the difference lies in concentration range: They used 5-26 mg/ml while the author used 2-10 mg/ml. They overlook the difference of concentration dependences of I(0)/C's and Rg's: the concentration dependence differs with the amount of bound Ca^{2+}. At dense concentrations apparently I(0)/C and Rg increases with increasing Ca^{2+} concentration however intrinsic Rg and I(0)/C at infinitely diluted concentration does not increase as clearly indicated in Figures 10 and 11. At low concentration the Rg decreases with increasing Ca^{2+} at 6.4 mg/ml. They performed SAXS experiments effectively at only three points and used the points at high protein concentration where I(S) of the inner part is distorted by the interparticle interference effect. The other reason is probably the optics. The optics

they used distort the SAXS profile in the small S region because a serious smearing of profile cannot be avoided for a camera length of 56.1 cm with a 5-mm-wide detector aperture. Thus, the intrinsic Rg of Tn-C in the Ca^{2+}-free state is much smaller than ours. Lyophilized Tn-C was used by Hubbard et al., so it may not have been intact. They also used a different ion in the sample buffer, NaCl instead of KCl.

Heidorn and Trewhella studied the SAXS from Tn-C in the presence of Mg^{2+}. Mg_2Ca_2Tn-C was also contaminated with dimer and only Mg_2Ca_0Tn-C was studied. Extrapolation of Rg^2 yielded a Rg of 23.0 Å, which is smaller than our result. Their protein concentration range (13-52 mg/ml) was apparently too high to extrapolate to infinite dilution; in the concentrations the inner part of SAXS profiles were distorted by the strong particle interference effect. The maximum length from the P(r) function consequently tends to be smaller. Moreover, the X-ray intensity was so weak that they only could obtain very noisy profiles even by exposures of several hours at 23℃.

The other feature of the present results is the analysis. Heidorn and Trewhella and Hubbard et al. determined the radius of gyration of Tn-C and the maximum length for the P(r) function. These two parameters are relevant. In contrast, my analysis is based on the characteristic structure of Tn-C. I herein present the radius of gyration of the domains and the distance between them, which yield the useful, detailed information that the domain of the high affinity sites (C-domain) becomes more compact and that the two domains get closer together (i.e., the molecule contracts along its major axis) upon Ca^{2+} binding.

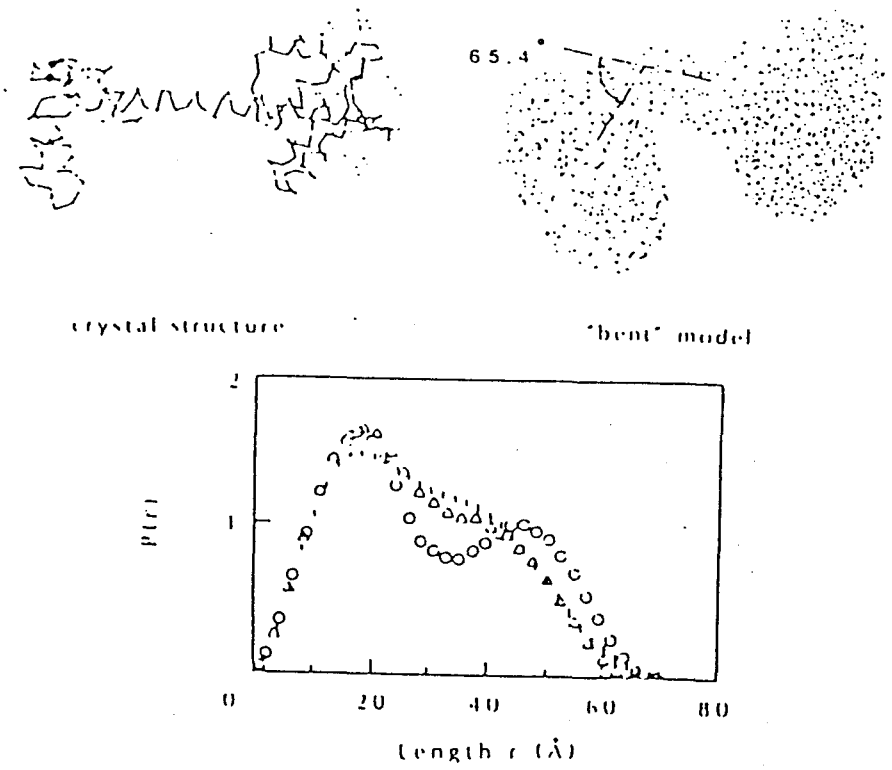

Figure 31: P(r) functions calculated for Tn-C with the uniform ellipsoid model presented by Heidorn and Trewhella (31). Crystal structure (○), the bent model (△), and experimental curve for Mg_2Ca_0Tn-C (|). Crystal structure and their bent model were illustrated above.

6. Comparison of the Structure in Solution with that in Crystal

First of all we can compare our data with those of crystal structure analysis (7-10). Crystallized Tn-C carries two Ca^{2+} ions in the C-domain, so that it corresponds to Ca_2Tn-C. The main difficulty in calculating SAXS profile from crystalline structure is the evaluation of the solvent. The intensity-calculation program made by Mr. Shin-i considers the effect of solvent inaccessible volume. The calculated intensity from crystalline structure of lysozyme was identical with the experimental profiles (49). In case of Tn-C, the main characteristic hump from crystalline structure was common to the SAXS data although the difference between them was apparent: the SAXS profile shifted to smaller angles. First peak in P(r) function of crystalline structure located at 17 Å, which was smaller than our result but the second peak was almost at identical length (Figures 12 and 18). The same observation was verified in both TR1C and TR2C in Figure 25. This indicates size of the domain in solution is larger than that in crystal. Physical parameters also suggest above. From the amino acid coordinates of Tn-C, Rg, $\overline{Rg}_{N,C}$ and r_{NC} were 22.9 Å, 12.5 Å and 41.7 Å, respectively. The Rg and $\overline{Rg}_{N,C}$ were smaller than that of solution. On the basis of several lines of studies the conformation of the domain can not be so different. The difference is probably attributable to the associated water. The other possibility is the difference in the structures of the domains, caused by electrostatic repulsive forces between the ionized groups.

The 52% α-helicity in solution determined by CD measurement is smaller than the value in the crystalline state (67%) (7,14). A potentiometric titration study also indicated the possibility of an expanded Tn-C structure at neutral pH (13). Satyshur et al. themselves admit the effect of pH on protein structure since the growth and stability of the crystals are very sensitive to pH (10).

The 14.8 Å of $\overline{Rg}_{N,C}$ corresponds to a radius of a uniform sphere of 19.1 Å, so that the separation of the two domains may not be so clear as in the crystalline state when the high affinity sites are occupied. The characteristic of P(r) function is accordant with above; the second peak at 40 Å in P(r) is more clearer when the separation of two domains becomes distinct. The finding is also reported by other SAXS studies (30,31). This structure could make it possible for the N- and C-domains to interact with each other, as suggested by other methods (see INTRODUCTION).

7. Changing Mechanism for the Protein Compaction

If the Tn-C molecule contracts along with main axis upon Ca^{2+} or Mg^{2+} binding, the question is how it can occur.

In crystalline structure the linker helix is exposed to solvent. The α-helix is usually unstable in solvent medium, in the case of Tn-C the complicated electrostatic interaction between side chains of helix keeps it. The isotropic temperature factor, which gives an indication of the regions with more or less conformational flexibility in the molecule, is high

in the region of linker helix (9). The increase in pH could bring about the flexibility of the helix. Both Satyshur and Herzberg considered this hypothetical conformation change in the linker region on Ca^{2+} binding would bring about a change in the relative deposition of the two domains (9,10). Heidorn et al. showed that hypothetical rotation around the center of the linker helix could explain their SAXS results. Recently Xu and Hitchcock-DeGregori explored a Tn-C mutant in which residues 91-93 (Lys-Gly-Lys) in the linker helix were deleted (58). It differs in function from wild-type Tn-C in the conformational change upon Ca^{2+} binding and its interaction with Tn-I. The region near Gly-92, therefore appears to play an important role in molecular contraction.

ACKNOWLEDGMENT

The author is sincerely grateful to Dr. Tatzuo Ueki and Professor Toshio Mitsui for their valuable discussions. The author is indebted to Drs. Shozo Iida of Nagoya University and Katsuzo Wakabayashi of Osaka University for their many useful suggestions. I further thank Drs. Katsumi Kobayashi of Photon Factory, Yoji Inoko of Osaka University, and Mikio Kataoka of Tohoku University for their help in SAXS experiments at the Photon Factory. This work has been performed under the approval of the Photon Factory Program Advisory Committee (Proposal No. 87-033).

APPENDIX

A. Analysis of small-angle Scattering Intensity Based on the Dumbbell Structure

A.1. Small-Angle Scattering Intensity based on the Dumbbell Structure: Small-Angle Region

In crystalline state, the Tn-C molecule consists of N-terminal domain (N-domain), C-terminal domain (C-domain) and a linker helix . N-domain includes the first 85 amino-acid residues and C-domain comprises the last 66 residues. The linker helix of 12 residues can be approximated as a short, thin rod whose scattering profile becomes pronounced in much higher scattering angle region than the region dealt with in the present paper. The number of electrons included in this rod is smaller compared with that in the domains (12 residues out of total of 162 amino acid residues) (7,8), so that the intensity of cross-terms between the rod and the domains is assumed to be small. Neglecting the linker helix, the model structure is well approximated by the two domains as

$$\begin{aligned} \rho(\vec{r}) &= \rho_N(\vec{r}) + \rho_c(\vec{r}) + \rho_h(\vec{r}) \\ &\simeq \rho_N(\vec{r}) + \rho_c(\vec{r}) \end{aligned} \qquad \text{(A-1)}$$

where $\rho_N(\vec{r})$, $\rho_c(\vec{r})$ and $\rho_h(\vec{r})$ are electron densities of the N-domain, C-domain and linker helix, respectively. Although $\rho_N(\vec{r})$ and $\rho_c(\vec{r})$ are not spherically symmetric, they can be assumed to be so if the analysis is confined in the small angle region, S

$\leqq$ 0.03 $\mathring{A}^{-1}$. This assumption is supported by SAXS experiments from tryptic fragments of Tn-C. In these experiments, it was shown that the scattering intensities were expressed in the form of Gaussian function up to S = 0.03 $\mathring{A}^{-1}$ (see Figure 20). Thus, $\rho_N(\vec{r})$ and $\rho_C(\vec{r})$ can be written as spherically symmetric $\rho_N(r)$ and $\rho_C(r)$ since the MW of these domains are less than 10,000 daltons. $\rho(\vec{r})$ can be written by using $\rho_N(r)$, $\rho_C(r)$ and the positional vectors of the centers of these domains, $\vec{r}_N$ and $\vec{r}_C$, as

$$\rho(\vec{r}) = \rho_N(r) * \delta(\vec{r} - \vec{r}_N) + \rho_C(r) * \delta(\vec{r} - \vec{r}_C), \qquad (A\text{-}2)$$

where * denotes a convolution operation and $\delta(\vec{r})$ the Dirac delta function (59).

After Fourier transforming $\rho(\vec{r})$ and taking the spherical average of the square of the Fourier transform, I(S) is given as

$$I(S) = f_N^2(S) + f_C^2(S) + 2\, f_N(S) f_C(S) \mathrm{sinc}(2\pi r_{NC} S), \qquad (A\text{-}3)$$

where $\mathrm{sinc}(X) = \sin(X)/X$ and $r_{NC} = |\vec{r}_N - \vec{r}_C|$. In Eq (A-3),

$f_N^2(S) = \int_N \rho_N(r)\mathrm{sinc}(2\pi Sr)dr = n_N^2 \exp[-(4\pi^2/3)Rg_N^2 S^2]$

and

$f_C^2(S) = \int_C \rho_C(r)\mathrm{sinc}(2\pi Sr)dr = n_C^2 \exp[-(4\pi^2/3)Rg_C^2 S^2]$.

n_N and n_C are the effective numbers of electrons belonging to the N- and C-domains, respectively, and Rg_N and Rg_C are their radii of gyration.

The difference in scattering intensity of domains, between the cases in which the domains are treated separately and in which they are averaged, is estimated to be about 0.1 % at S =

0.0 and 2 % at S = 0.03 A^{-1}. Thus, the averaging of scattering factors for the domains does not lead to a serious error and hence the average scattering factor, f(S) is written as follows,

$$f^2(S) = \bar{n}_{N,C}{}^2 \exp[-(4\pi^2/3)\overline{Rg}_{N,C}{}^2 S^2]. \qquad (A\text{-}4)$$

In Eq (A-4) $\bar{n}_{N,C}$ is the average of the effective number of electrons of the two domains, and $Rg_{N,C}$ is the average radius of gyration defined as (60)

$$\overline{Rg}_{N,C}{}^2 = \{n_N/(n_N + n_C)\}\, Rg_N{}^2 + \{n_C/(n_N + n_C)\}\, Rg_C{}^2 . \qquad (A\text{-}5)$$

Then, we have

$$I(S) = 2\, f^2(S)\, \{\, 1 + \mathrm{sinc}(2\pi r_{NC} S)\, \}. \qquad (A\text{-}3')$$

After expanding sinc(X) in the Taylor series at X = 0, and approximating the series with an exponential function, Eq (A-3') is expressed in the Guinier form,

$$I(S) = 2\, f^2(S) \exp[-(4\pi^2/3)(r_{NC}{}^2/4)S^2]$$
$$= 2\bar{n}_{N,C}{}^2 \exp[-(4\pi^2/3)\{\overline{Rg}_{N,C}{}^2 + (r_{NC}{}^2/4)\}S^2]. \qquad (A\text{-}6)$$

This is valid in a very small angle region, and what we obtain from the plot of ln{I(S)} <u>vs.</u> S^2 , <u>i.e.</u>, the radius of gyration of whole Tn-C molecule, Rg, is ;

$$Rg^2 = \overline{Rg}_{N,C}{}^2 + r_{NC}{}^2/4. \qquad (A\text{-}7)$$

If $\overline{Rg}_{N,C}$ is known, we can get the value of r_{NC}.

A.2. Small-Angle Scattering Intensity Based on the Dumbbell Structure : The Linear Region in ln{I(S)/S} vs. S^2 plot

I will show that $\overline{Rg}_{N,C}$ is estimated from the linear region in ln{I(S)/S} *vs.* S^2 plot. The term, $1 + \mathrm{sinc}(2\pi r_{NC} S)$, in Eq (A-3') is called an interference term. The "hump" observed in SOXS profile (Figure 7) is understood as that arising from this term. The position of the hump gives, in principle, the value of r_{NC}, but it is difficult to determine its accurate position since it appears only as a shoulder.

I discuss the appearance of the $\overline{Rg}_{N,C}$ as follows. If the function sinc(X) is expanded in Taylor series around $X = 2\pi$ up to the first and second terms, we have

$$\mathrm{sinc}(2\pi r_{NC} S) = (r_{NC} S - 1) - (r_{NC} S - 1)^2. \qquad \text{(A-8)}$$

Near $S = 1/r_{NC}$, the second term is taken to be very small and I(S) can be written using Eq (A-4) as

$$I(S) \simeq 2 f^2(S)(r_{NC} S)$$
$$= 2\bar{n}_{N,C}^2 \exp[-(4\pi^2/3) \overline{Rg}_{N,C}^2 S^2](r_{NC} S). \qquad \text{(A-9)}$$

Dividing I(S) by S and taking logarithm of {I(S)/S}, Eq (A-9) gives,

$$\ln\{I(S)/S\} = \ln\{2\bar{n}_{N,C}^2 r_{NC}\} - (4\pi^2/3)\overline{Rg}_{N,C}^2 S^2. \qquad \text{(A-10)}$$

Eq (A-10) indicates that the ln{I(S)/S} *vs.* S^2 plot must have a linear region around $S = 1/r_{NC}$, and the slope of the straight line in the plot yields the radius of gyration of domains, $\overline{Rg}_{N,C}$

(Eq (A-7)). Figure 12 shows such plots for Tn-C solutions and indicates that the linear region is recognized for all concentrations of Ca^{2+}.

REFERENCES

1. Ebashi, S., Wakabayashi, T. & Ebashi, F. (1971). J. Biochem. 69, 441-445.
2. Leavis, P.C. & Gergely, J. (1984) CRC Crit. Rev. Biochem. 16, 235-305
3. Zot, A., S. and Potter, J.D. (1987) Ann. Rev. Biophys. Biophysic. Chem. 16, 535-559
4. Collins, J.H., Greaser, M.L., Potter, J.D., & Horn, M.I. (1977) J. Biol. Chem. 242, 6356-6362
5. Potter, J.D. & Gergely, J. (1975) J. Biol. Chem. 250, 4628-4633
6. Leavis, P.C., Rosenfeld, S.S., Gergely, J., Grabarek, Z., & Drabikowski, W. (1978) J.Biol.Chem. 253, 5452-5459
7. Herzberg, O. & James, M.N.G. (1985) Nature 313, 653-659
8. Sundaralingam, M., Bergstrom, R., Strasburg, G., Rao, S.T., Roychowdhury, P., Greaser, M., & Wang, B.C. (1985) Science
9. Herzberg, O. & James, M.N.G. (1988) J. Mol. Biol. 203, 761-779
10. Satyshur, K.A., Rao, S.T., Pyzalska, D., Drendel, W., Greaser, M., & Sundaralingam, M. J.Biol.Chem. 263, 1628-1647
11. Krestinger, R.H., & Nockholds, C.E. (1973) J.Biol.Chem. 248, 3313-3326
12. Babu, Y., Sack, S., Grenhough, T., Bugg, C., Means, A. & Cook, W. (1985).Nature, 315, 37-40.
13. Iida, S. (1979) J. Biochem. 86, 733-743
14. Kawasaki,Y. & van Eerd, J.P. (1972) Biochem.Biophys.Res.Commun. 47, 898-905
15. van Eerd, J.P. & Kawasaki, Y. (1972)

Biochem.Biophys.Res.Commun. 47, 859-865

16. Murray, A.C. & Kay, C.M. (1972) Biochemistry, 11, 2622-2627
17. Byers, D.M. & Kay, C.M. (1982) Biochemistry 21, 229-233
18. Mani, R.S., McCubbin, W.D., & Kay, C.M. (1974) Biochemistry, 24, 5003-5007
19. Levine, A., Mercola, D., Coffmcn, D., & Thornton, J.M. (1977) J.Mol.Biol 115, 743-760
20. Seamon, K.B., Hartshorne, D.J., & Bothner-By, A.A. (1977) Biochemistry, 16, 4039-4045
21. Iio, T. & Kondo, H. (1981) J. Biochem. 90, 163-175
22. Cohen, S.M., & Burt, C.T. (1977) Proc. Natl. Acad. Sci. USA 74, 4271-4275
23. Levine, B.A., Thornton, J.M., Fernandes, R., Kelly, C., & Mercola, D. (1978) Biochim. et Biophys. Acta, 535 11-24
24. Iida, S. (1988) J.Biochem. 103, 482-486
25. Wang, C.L.A., Zhan, Q., Tao, T., & Gergely, J. (1987) J. Biol. Chem. 262, 9636-9640
26. Grabarek, Z., Leavis, P.C., & Gergely, J. (1986) J.Biol.Chem. 261, 608-613
27. Wang, C.L.A. & Gergely, J. (1986) Eur.J.Biochem. 154, 225-228
28. Tsalkova, T.N. & Privalov, P.L. (1985) J.Mol.Biol. 181, 533-544
29. Tsuda, S., Hasegawa, Y., Yoshida, M., Yagi, K., & Hikichi, K. (1988) Biochemistry 27, 4120-4126
30. Hubbard, S.R., Hodgson, K.O., & Doniach, S. (1988) J. Biol. Chem. 263, 4151-4158

31. Heidorn, D.B. & Trewhella, J. (1988) Biochemistry 27, 909-915

32. Cheung, H.C., Wang, C.K., & Garland, F. (1982) Biochemistry 21, 5135-5142

33. Wang, C. K. & Cheung, H.C. (1986) J. Mol. Biol. 190, 509-521

34. Ueki, T., Inoko, Y., Kataoka, M., Amemiya, Y. & Hiragi, Y. (1986). J. Biochem. 99, 1127-1136.

35. Fujisawa, T., Ueki, T., Inoko, Y., & Kataoka, M. (1987) J. Appl. Cryst. 20, 349-355

36. Margossian, S.S. & Stanford, III, W.F. (1982) J. Biol. Chem. 257, 1160-1165

37. Ebashi, S., Wakabayashi, T., & Ebashi, F. (1971) J. Biochem. 69, 441-445

38. van Eerd, J.P. & Kawasaki, Y. (1973) Biochemistry 12, 4972-4980

39. Drabikowski, W., Grabarek, Z., & Barylko, B. (1977) Biochim. et Biophys. Acta, 90 216-224

40. Perrin, D.D. & Sayce, I.G. (1967) Talanta 14, 833-842

41. Levinson, B.L., Pickover, C.A., & Richards, F.M. (1983) J. Biol. Chem. 258, 10967-10972

42. Conrad, H., Mayer, A., Thomas, H. P. & Vogel, H. (1969). J. Mol. Biol. 41, 225-229.

43. Ueki, T., Izumi, Y., Tagawa, H., Hiragi, Y., Kataoka, M., Muroga, Y., Matsushita, T., & Amemiya, Y. (1984) personal communication

44. Kohra, K. (1984) In KEK Progress Report 83-1, Photon Factory Activity Report 1982/83, pp. V-8-9, V-29, V-35, KEK, Tsukuba,

Japan

45. Guinier, A. & Fournet, G. (1955) Small-Angle Scattering of X-rays, New York: Jhon Wiley
46. Glatter, O. (1977) Acta phys. Austriaca 47, 83-102
47. Glatter, O. (1977) J. Appl. Cryst. 10, 415-421
48. Pickover, C.A. & Engelman, D.M. (1982) Biopolymers, 21, 817-831
49. Shin-i, T. (1988) In graduation thesis for Osaka University
50. Atkins, P.W. In Physical Chemistry, London: Oxford University Press
51. Glatter,O. (1982) In Small Angle X-ray Scattering, Academic, New York
52. Eisenberg, H. (1981) Q.Rev.Biophys. 14, 141-172
53. Pilz, I., Goral, H., Hoyaerts, M., Lomtie, R., & Witters, R. (1980) Eur. J. Biochem. 105, 539-543
54. Seaton, B.A., Head, J.F., Engelman, D.M., & Richards, F.M. (1985) Biochemistry 24, 6740-6743
55. Zaccai, G. & Jacrot, B. (1983) Ann. Rev. Biophys. Bioeng. 12, 139-157
56. Serdyuk, I.N., Tsalkova, T.N., Svergun, D.I., & Izotovc, T.D. (1987) J.Mol. Biol. 194, 126-128
57. Marshall, A.G. (1978) In Biophysical Chemistry, John Wiley & Sons
58. Xu, G.Q. and Hitchcock-DeGregori, S.E. (1988) J.Biol.Chem. 263, 13962-13969
59. Vainstein, B.K. (1966) In Diffraction of X-rays by Chain Molecules, pp24-31, Amsterdam, Elsevier

60. Serdyuk, I.L. & Federov, B. A. (1973). J. Pol. Sci. (Pol. Lett. Ed.) 11, 645-649.